MULTILAYER SCALABLE COUPLER WITH HIGH DIRECTIVITY

A Thesis
Presented to
The Academic Faculty

by

Nina Popovic Basta

In Partial Fulfillment
of the Requirements for the Degree
Master's Thesis in the
School of Electrical and Computer Engineering

Georgia Institute of Technology
August 2015

MULTILAYER SCALABLE COUPLER WITH HIGH DIRECTIVITY

Approved by:

Professor Alenka Zajić, Advisor
School of Electrical and Computer Engineering
Georgia Institute of Technology

Professor John Papapolymerou
School of Electrical Engineering
Georgia Institute of Technology

Professor Manos M. Tentzeris
School of Electrical Engineering
Georgia Institute of Technology

Date Approved: July 21 2015

ACKNOWLEDGEMENTS

First and foremost, I would like to thank my advisor, Prof. Alenka Zajić for the opportunity to be her graduate student, the research funding and for her invaluable technical guidance. I am grateful to members of my thesis committee, Prof. Manos Tenzeris and Prof. John Papapolymerou, for their time and support.

I would also like to thank the strong network around me, especially my parents (Zoya and Dana), sisters and Alex. They have not only helped me during my year and a half in graduate school, but have supported me my entire life, always providing unconditional love and encouragement. This thesis would not have been possible without the company of my friends and colleagues from Georgia Tech, including but not limited to Michael, Brittney, and Jon, as well as my friends from undergraduate days at McGill University, especially Ian, Josh, Marwan, and Raissa.

This thesis is dedicated to my maternal grandmother Nana Olja for always believing in me, and the memory of my grandfather Deda Branko who was the first one to show me that engineering can be fun.

Contents

ACKNOWLEDGEMENTS . . . . . **iii**

LIST OF TABLES . . . . . **vi**

LIST OF FIGURES . . . . . **vii**

SUMMARY . . . . . **x**

I INTRODUCTION **1**

1.1 Motivation and Scope 1

1.2 Thesis Outline 4

II BACKGROUND **6**

2.1 Summary of Commonly Used Couplers 6

2.1.1 Waveguide Couplers 8

2.1.2 Coupled-Line Couplers 11

2.1.3 Interconnected quarter-wave transmission line couplers 13

2.1.4 Broadside Couplers 17

2.2 Couplers in Literature 18

III COUPLED-LINE THEORY **21**

3.1 Edge Coupling 21

3.1.1 Electrically-Short Coupled-line Section 25

3.1.2 Electrically-long Coupled-line Section 27

3.1.3 Even and Odd Mode Impedances 28

3.2 Broad-side Coupling 30

3.3 Combined Broadside and Edge Coupling 31

IV SIMULATION AND MEASUREMENT **34**

4.1 Procedure Background 34

4.1.1 Design Overview 35

4.1.2 Simulation Tools 35

4.1.3 Fabrication Specifications 36
4.1.4 Calibration 38
4.2 Coupler Design 38
4.2.1 Simulation 38
4.2.2 Measurement 43
4.2.3 Discussion 45
V CONCLUSIONS AND FUTURE WORK 51
REFERENCES 53

List of Tables

1 Specifications Behind Common Coupler Topologies. The isolation and coupling follow the definitions given in equations (1), (2), and (3). [44] 7

2 A Brief Review of Miniaturized, Multilayer or High Frequency Couplers in Literature 19

3 S-parameter definitions and their corresponding ideal values 24

4 Substrate characteristics valid for 1 GHz as well as fabrication limitations for OSH Park 36

5 Affects of dimensions adjustments on S-parameters. Dimensions are in mm and S-parameters are in dB and x's indicate the parameter has not changed from the initial value. 39

6 Fabricated coupler dimensions corresponding to those labeled in Fig. 20. All dimensions stay the same as frequency shifts except for the length. 42

7 Measured characteristic S-parameters of the coupler. 51

List of Figures

1 A simple illustration of NoC, the interconnection between cores (blue squares). The black lines are wire interconnects, the circles are the routers/switches, and the pink and orange are examples of possible paths for two different instructions. 2

2 A possible layout of transmission-line couplers connecting 4 cores in a processor. The green crosses represent switches that route the signals. The thick black lines represent 4 directional couplers, with P1 being the input port, P2 the through port, and ports P3 and P4 the coupled and isolated ports respectively. 3

3 A schematic of a coupler with the input, through, isolated, and coupled ports labeled; type of coupling not specified. 8

4 Examples of directional waveguide couplers (a) Bethe-hole coupler with fourth isolated port sealed [46] and the illustrations of wave generation [44]; (b) Schematic of basic Moreno coupler implemented with two slot apertures [17]; (c) (i) Geometry of a magic T coupler with propagation of waves when (ii) port 1 is the input port and (iii) port 2 is the input port. 10

5 Examples of coupled-line couplers (a) Basic topology of a Lange coupler with bond-wire placement shown [44]. (b) Schematic of a tapered coupled-line coupler [44] and multi-section coupled-line coupler [36]. 13

6 Examples of edge-side couplers (a) Branch line coupler schematic illustrating the impedance and phase shift correlated to each transmission line segment [51]. (b) Multiple rat-race topologies, [37] for the two on the left, and [21] for the one of the right. 14

7 Circuit reduction of a branch-line coupler when port 2 is shorted (a) the original branch-line coupler with transmission line lengths and impedances; (b) simplified when port 2 is shorted and; (c) further simplification where ports 3 and 4 are consolidated. 16

8 An illustration of a basic coplanar waveguide broad-side coupler [48]. A single coplanar waveguide with some width S and separation from ground W is separated by some h_1 above another coplanar waveguide. This system shows a symmetric system with ground above and below the coupler. 17

9 A simple illustration of a two line system and its (a) electric and (b) magnetic field coupling circuit setup. 22

10 Sketch of magnetic and electric field lines of two coupled lines for (a) even and (b) odd mode fields. The density of fields resulting from the different permittivities (ϵ_0 and ϵ_r) are visualized with the different number of lines. The bottom electrode is assumed to be at zero potential. 23

11 The layout of a four port microstrip coupler with a basic edge-side coupler orientation P1 is the input port, P2 is the through port, P3 is the coupled port and P4 is the isolated ports. The characteristic S-parameters outlined in Table **??** are calculated based on the propagating voltages. 23

12 Four port-coupler of some length L terminated with Z_0 at all ports. The top four-port illustrates capacitive coupling while the bottom diagram describes inductive coupling. 25

13 The even and odd mode capacitances decomposed into their individual components, where C_f, C'_f, C_{ga} and C_{gd} are the fringing capacitances. Many references use this model, e.g. [11]. 28

14 Cross-section of two-line, stripline, broad-side coupling system. The evaluation techniques are similar to those used for edge-side coupling. 30

15 (a) The AWR layout for a four-line multilayer coupler where the lines on separate layers are not connected. (b) S-parameters corresponding to this topology. S_{11}, S_{31}, and S_{41} are on the left axis while S_{21} is on the right axis. This geometry results in very poor matching at port 1, low coupling, and low directivity. 32

16 A transverse cross-section of a three-layer topology. The dashed lines indicate which of the coupled lines are connected with vias. The dielectric heights between the ground the coupled lines are not the same. The widths w_1 and w_2 as well as the separations s_1 and s_2 are variables used for optimization. 34

17 The simplest simulation in AWR for a three-layer, four-port coupler where the four lines are connected in diagonal. No additional transmission line or vias was included in the model. 38

18 S-parameters for simplest AWR model shown in Fig. 17 with $|S_{11}|$ and $|S_{41}|$ are on the left hand axis while $|S_{21}|$ and $|S_{31}|$ are on the right hand axis. The 3 dB coupler has isolation and return loss below 30 dB, specific values are shown by the markers. 40

19 2D simulation of coupler, similar to Fig. 17 with additional components to take the inductive and capacitive characteristics of both the vias and extra transmission lines into account. 41

20 The dimensions labeled are in Table 6 (a) The layout of one end of the coupler with blue for the top layer, purple for vias to ground, green for vias between first and second layer, and yellow for second layer. (b) Both fabricated couplers for 1 GHz (left) and 3 GHz (right) pictured with SMA connectors used for measurement. The only dimension that changes between the two couplers is their length. 42

21 Experimental set-up used to measure the S-parameters of the coupler. The Network Analyzer (N5224A) is connected using 50 Ω coaxial lines to two of the four ports on the coupler. The other two ports are connected to 50 Ω loads. 43

22 The measured S-parameters for the first design of the 1 GHz and 3 GHz coupler. All of these measurements were done using the standard calibration described earlier in this chapter. (a) 1 GHz, 3 dB coupler with -22 dB isolation and return loss. (b) 3 GHz, 3 dB coupler with -20 dB isolation and -24 dB return loss. 44

23 Simulation of awr and cst vs. measurement for the S-parameters of the 1 GHz coupler for the first coupler design. The first design in AWR, corresponding to Fig. 17 is designated with a dark black dotted line, the second design in awr, shown in Fig. 19 is the dashed dotted magenta line CST with a dashed blue line, and measured with a solid green line. 46

24 Simulation of awr and cst vs. measurement for the S-parameters of the 3 GHz coupler for the first coupler design. The first design in AWR, corresponding to Fig. 17 is designated with a dark black dotted line, the second design in awr, shown in Fig. 19 is the dashed dotted magenta line CST with a dashed blue line, and measured with a solid green line. 47

25 Evaluating the sensitivity of the 1 GHz coupler by adjusting different parameters of the coupler by 5% and 10%. The blue squares indicates parameters were altered by 5%, the pink circles are the S-parameters after 10% alteration, and the green triangle is the original data s-parameter value. S_{21} and S_{31} are both differ by less than 1 dB while S_{11} and S_{41} differ by only a few %. 49

26 Evaluating the stability of the 3 GHz coupler by adjusting different parameters of the coupler by 5% and 10%. The blue squares indicates parameters were altered by 5%, the pink circles are the S-parameters after 10% alteration, and the green triangle is the original data s-parameter value. 50

27 Schematic of power measurement calibration. With the device under testing (DUT) attached to a power source at port 1, power meter attached to port 1 to measure P1, and all other ports terminated in Z_0. 52

SUMMARY

This thesis addresses the design, analysis, and experimental validation of a high-directivity and high coupling microwave directional coupler. The motivating application is in broadband signal routing between cores of multi-core processors, where the delay of simple wire interconnects introduces unacceptable latency. The performance goals include scalability with frequency, a coupling coefficient of 3 dB, directivity larger than 40 dB, high return loss, low insertion loss below 3 dB at the center frequency, and small footprint.

The approach to this problem taken in the thesis is a combination of edge and broad-side coupling in a multi-layer, multi-conductor microstrip coupled-line system. The two coupling mechanisms between neighboring pairs of coupled lines, along with appropriate end interconnections, allow for reduced size and design that achieves equal propagation velocities for the different modes supported by the five-conductor guiding structure that contribute to coupling. To validate the approach, a coupler designed for operation at 1 GHz is demonstrated to have a isolation of - 22 dB with a coupling coefficient of 3 dB and a return loss of - 20 dB. The coupler is implemented on a FR-408 substrate with a permittivity of $\epsilon_r = 3.66$ and 1.17 mm and 0.17 mm thicknesses, and a total area of 12.65 cm^2. Three metalization layers are used in the design, with edge and broad-side coupled pairs of lines on the top two layers and diagonal end interconnects between the top and bottom lines. The coupler design is then scaled to 3 GHz by shortening the coupled-line length, and established -24 dB isolation, coupling of 3 dB, return loss of -20 dB, and has a total area of 6.9 cm^2.

The analysis of the coupler shows that full-wave electromagnetic modeling agrees

well with measurements and is necessary during the design process, while circuit analysis with built-in coupled-line models shows poorer agreement with experimental data. A tolerance analysis shows that the coupler performance is most sensitive to milling precision and separation between coupled-lines. Based on the measured and simulated results, it is shown that this type of coupler can be further scaled to higher frequencies and on-chip implementations for signal distribution in multi-core processors, or any other application where a number of components need to be interconnected with low latency and no reflection.

Chapter I

INTRODUCTION

1.1 Motivation and Scope

Couplers are electromagnetic components used for an assortment of applications with structural variations based on a few commonly used designs. The most important performance parameters include the insertion loss and coupling coefficient, which can range from 3 dB (half of input power coupled) to as low as -30 dB (0.1 % of power coupled). This thesis focuses on the design and fabrication of a multi-layer, scalable, highly directional coupler for the purpose of increasing communication bandwidth on-chip of a multi-core processor. The coupler is designed to operate at 1 GHz and then only the length is decreased so that the operation frequency shifts to 3 GHz.

Microprocessors have been evolving since their first commercial release in 1971 by Intel [14]. As consumer needs have increased to include multiple threads excuted in parallel (e.g. running muliple programs at once), more powerful processors are necessary. Instead of focusing on making one very powerful processor, multiple cores on one processor has been discussed and implemented [13], [45]. The problem of designing optimal multi-core processors has both a hardware [20] and software [14], [29], [3] perspective and they must be compatible with one another.

Traditionally core-to-core communication was "point-to-point" within a chip, however as one can imagine this becomes increasingly slow and unmanageable as the number of cores and their connections increase. An optimal set of software commands uses each core without duplicating jobs and minimizes the distance from required ports, such as instruction level parallelism (ILP) [14]. There are a variety of possible physical implementations that are compatible with the software, the most common

of which is illustrated in Fig. 1, the network on chip (NoC) is designed to deal with scalability issues. A NoC is an interconnect structure that contains a series of routers or switches, controlled to optimize the propagation delay between cores as a command is being executed [29]. One of the problems with this and other designs, is the execution time is limited by the speed of the interconnections. In the frequency domain, the bandwidth of the NoC architecture limits the communication bandwidth between cores.

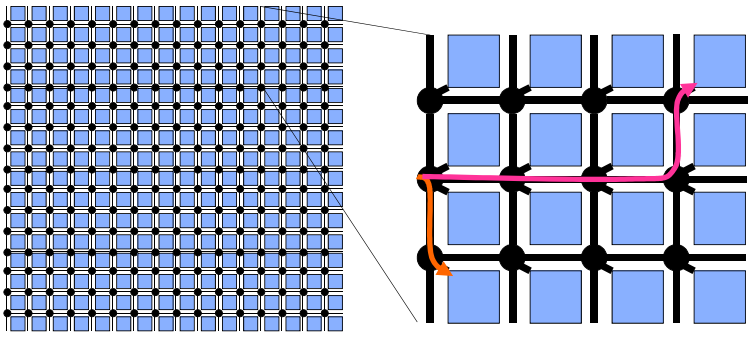

Figure 1: A simple illustration of NoC, the interconnection between cores (blue squares). The black lines are wire interconnects, the circles are the routers/switches, and the pink and orange are examples of possible paths for two different instructions.

In an attempted to increase the communication bandwidth of interconnects between the cores, this thesis addresses a directional coupler as a component for a traveling-wave transmission-line based interconnect network.

Fig. 2 illustrates an example of how the coupler could be incorporated into a four core system. The signal would propagate along an outer ring and couple to each coupler until a control signal to the switch disabled the connection. The symmetry of the coupler allows any of the ports to be the incident port, therefore both ports 1 (P1) and 4 (P4) can be used as the transmitting ports while ports 3 (P3) and 2 (P2) are the respective receiving ports.

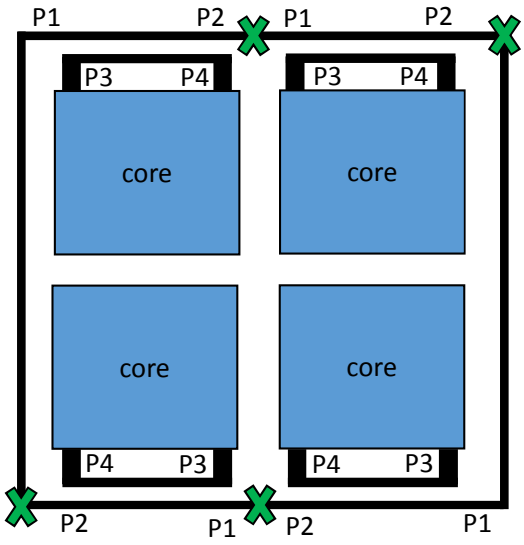

Figure 2: A possible layout of transmission-line couplers connecting 4 cores in a processor. The green crosses represent switches that route the signals. The thick black lines represent 4 directional couplers, with P1 being the input port, P2 the through port, and ports P3 and P4 the coupled and isolated ports respectively.

A coupler used for core-core communication on chip, requires high isolation (-20 dB) and low return loss (-20 dB). The coupler in this thesis is designed to divide the power equally between ports 2 and 3, however the structure of this coupler is capable of achieving coupling coefficients between 3 dB and 7 dB. This means that a coupler with the same structure and different coupling coefficients can be incorporated into a processor controlling the division of power along the main coupling line. This changeable coupling could be useful to optimize the hardware and software design of the transmission-line based interconnect network.

Other conventional couplers cannot be used for this application because they do not satisfy all of the parameters at once. For example, commonly used couplers either have low coupling (e.g. a single section coupled-line coupler), incompatible geometry are not planar (e.g. Bethe-hole), narrow bandwidth (e.g. multi section), or low

directivity (e.g. branch-line coupler). Other couplers described in published literature such as combinations or hybrids of commonly used couplers, multilayer couplers, and miniaturized couplers also cannot achieve all performance metrics while remaining scalable in frequency and being compatible with semiconductor fabrication.

Although this thesis focuses on designing a coupler for computer interconnection application, a coupler with high directionality, large bandwidth, scalability, and high coupling can be used in a variety of systems. The introduction of a coupler in miniaturized systems has increase the speed of signal propagation for real-time measurement and simplification of the fabrication process. For example, couplers have been implemented on on-chip measurement systems, such as a VNA [38].

1.2 Thesis Outline

This thesis is organized as follows;

- Chapter 2 summarizes commonly used couplers and their coupling mechanism. There are four groups of couplers based on mechanisms of coupling; waveguide, coupled-line couplers, interconnected quarter wavelength transmission line couplers (transmission line couplers) and broad-side couplers. Waveguide couplers and broad-side couplers are three-dimensional structures fabricated using waveguide and microstrip or coplanar waveguide respectively. Coupled-line couplers and transmission line couplers are planar structures made from microstrip or coplanar waveguide that rely on even-mode and odd-mode impedances and transmission line length respectively.

  None of the commonly used couplers alone have the characteristics required for the on-chip multi-core processor interconnections. There are many couplers in literature, some of which are discussed in this chapter, that are either miniaturized, scale with increased frequency, or have optimized directivity and insertion loss. In contrast the coupler in this thesis optimizes for all four characteristics

simultaneously as well as scaling in frequency by only adjusting length.

- Chapter 3 provides a transmission-line based theory as theoretical background for understanding coupler operation. A theoretical discussion of transmission-line based electromagnetic couplers is provided, giving both an insight into the physical operation and a mathematical description based on even and odd mode propagation.

  The coupler in this thesis uses both edge-side and broad-side coupling in a multil-layer microstrip architecture that is optimized for -20 dB isolation and return loss and 3 dB coupling. Similarly to the Lange coupler, the orientation of the four lines directly correlates to the functionality of the coupler. Several of these orientations are discussed and the optimal connection is found to be diagonal between lines on two different layers.

- Chapter 4 presents a specific design and experimental validation.

  The fourth chapter is a discussion of the design process. This chapter includes fabrication, calibration, design overview, simulations, measurements, and comparison. The fabrication capabilities as well as the measurement capabilities restrict the dimensions of the coupler, including separation between coupled-lines, port size, and dielectric ratios. The method of calibration SOLT is briefly described and an overview of fabrication tolerances is introduced. AWR and CST were used to optimize the coupler's dimensions with multiple models. An experimental prototype based on the CST 3D simulations is fabricated and measured data compared to simulations. In addition, a tolerance analysis is briefly discussed where physical dimensions of the coupler are adjusted by $\pm 5\,\%$ and $\pm 10\,\%$.

- Finally the last chapter concludes with some discussions and directions for future work.

Chapter II

BACKGROUND

2.1 Summary of Commonly Used Couplers

Coupling is the phenomenon of transferring energy from one system to another. In electrical systems coupling can either be used to perform certain functions or is viewed as an unwanted phenomenon in the case of signal interference, such as crosstalk. It can be used for multiple applications including near-field power transfer or in RF electronic components. Mixers, amplifiers, attenuators, power combiners, power dividers, refractometers etc. are all commonly used RF front-end circuit components that manipulate signals or power by coupling. This section gives an overview of various types of directional couplers.

Directional couplers are passive electromagnetic components with four ports: isolated, coupled, through, and input port, drawn in Fig. 3. They can be fabricated using stripline, waveguide, coax, coplanar waveguide (CPW), and microstrip. Table 1 gives an overview of the most commonly used couplers and outlines their capabilities with respect to coupling, isolation, bandwidth, and phase. The coupling, directivity, and isolation can be defined as;

$$C = 10\log\frac{P_1}{P_2} = -20\log|S_{31}|\,dB\ , \tag{1}$$

$$D = 10\log\frac{P_3}{P_4} = -20\log\frac{|S_{31}}{S_{41}}|\,dB\ , \tag{2}$$

$$I = 10\log\frac{P_1}{P_4} = -20\log|S_{41}|\,dB = C + D\ , \tag{3}$$

where the coupling factor represents the fraction of power coupled to the output port, directivity and isolation indicates the couplers capability of isolating forward from backward traveling waves and the ideality of the coupler.

Table 1: Specifications Behind Common Coupler Topologies. The isolation and coupling follow the definitions given in equations (1), (2), and (3). [44]

Coupler	**Coupling**	**Isolation**	**Bandwidth**	**Phase**
Bethe-Hole (waveguide)	∘ 10 to 20 dB for single hole ∘ related to directivity and physical parameters	∘ 30 dB single hole ∘ adjusted with angle, hole number, dimension, and placement	∘ broadband, covers full bandwidth with 2 apertures	∘ depends on hole number and placement
Moreno (waveguide)	∘ 10 to 20 dB ∘ related to directionality	∘ 30 dB ∘ adjusted with hole shape, separation, and placement	∘ usually narrowband ∘ shown to be 75% [17]	∘ depends on aperture orientation and shape
Magic T (waveguide)	∘ 3 dB ∘ highly dependent on fabrication	∘ 50 dB ∘ highly dependent on fabrication	∘ wide bandwidth (octave or more)	∘ 180 ° phase difference incident on port 4 ∘ in phase power split incident on port 1
Short-slot hybrid (waveguide)	∘ 3 dB ∘ shifts from coupling results in power unbalance	∘ 30 dB	∘ 15% bandwidth	∘ ports 2 and 3 90° out of phase
Lange Coupler (coupled-line)	∘ 3 dB	∘ 30 dB	∘ octave of bandwidth	∘ ports 2 and 3 90° out of phase
Coupled Line Coupler (coupled line)	∘ 10 to 15 dB	∘ 20 dB	∘ a decade or more	∘ 180° hybrid
Rat Race (ring hybrid) (interconnected)	∘ 3 dB	∘ 20 dB ∘ affected by section impedance/length and load mismatch	∘ 30% bandwidth when directivity is 20dB ∘ comes at expense of isolation	∘ ports 2 and 3 180° out of phase
Branch-line (interconnected)	∘ 3 dB	∘ 15 dB ∘ affected by section impedance/length and load mismatch	∘ 10-20% bandwidth ∘ bandwidth can be increased by adding sections ∘ bandwidth increased with loss	∘ port 2 and 3 in quadrature (90°)

Classical coupler topologies can be divided into four basic groups based on their coupling mechanisms; waveguide couplers, coupled-line couplers, interconnected quarter wavelength transmission line couplers, and broad-side couplers. Waveguide couplers (Bethe-hole, Moreno, magic T, and short-slot couplers) manipulate geometry and apertures between waveguide lines to force interactions between propagating waves. Coupled-line couplers and interconnected quarter wavelength transmission line couplers are fabricated using quasi-TEM guiding structures. Coupled-line couplers take advantage of the different even-mode and odd-mode velocities resulting from these quasi-TEM modes, while interconnected quarter wavelength transmission line couplers use their geometry to compensate for these even-mode and odd-mode velocities and impedances. Broad-side couplers works as large capacitors, the fields are focused in the dielectric between the two lines. A more in-depth discussion on even-mode and odd-mode waves is presented in the next chapter.

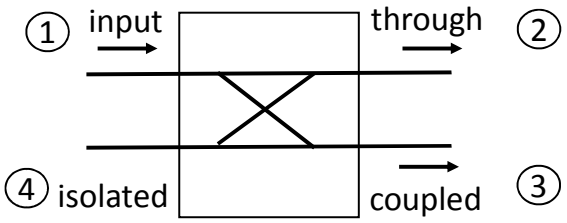

Figure 3: A schematic of a coupler with the input, through, isolated, and coupled ports labeled; type of coupling not specified.

2.1.1 Waveguide Couplers

Rectangular metallic couplers are four-port components that use apertures between two waveguides and guide geometry to create interactions between waves propagating in both guides. Each waveguide coupler uses apertures and geometry differently, as seen in Fig. 4. Bethe-hole, Moreno, and short-slot couplers operate using single or multiple apertures that can be modeled by electric and magnetic dipole moments [44] [46]. By modeling the apertures, it is relatively straight forward to design for

a specific coupling coefficient. A magic T is also a three-dimensional waveguide structure, however it uses geometrically orthogonal waveguides to alter the phase and propagation of waves at the intersection of the four waveguide lines.

The basic Bethe-hole coupler consists of two rectangular metallic waveguides that are coupled together through a few apertures at a given distance from each port. Lets say there are only two apertures quarter of a wavelength apart at the design frequency. When a wave is incident on port 1 (see Fig. 4a as a reference) a small amount of the propagating waves leaks through the apertures into the second waveguide. Both the coupled wave and initial wave keep propagating along the line. The forward propagating wave coupled through the first apertures adds in phase with the coupled wave from the second aperture and output at the coupled port. The two backward propagating waves from apertures 1 and 2 cancel in phase at the isolated port. Additional skew and apertures can be introduced to increase coupling, directivity, as well as bandwidth. When more than one aperture is used in the system, the coupling coefficient will scale linearly with the number of apertures [31] [46]. This coupler is easily modeled using dipoles or monopoles as equivalent sources for each aperture, and the resulting S-parameters can easily be manipulated using size, positioning, number of apertures, and skew between the waveguide lines. However, the coupling, which ranges from 10 - 20 dB, and directivity are a function of frequency. When the coupler is optimized using skew and apertures, the fabrication and even the realization (when skew is introduced) of the coupler becomes difficult.

Moreno crossed-guide couplers are similar to Bethe-hole couplers in the fact that they consist of two, aperture coupled, waveguide sections. However, they have a fixed 90° skew where the aperture size, shape (most commonly the apertures are crosses, however they can be slots as shown in Fig.4b), and separation are altered to change bandwidth, directivity, loss, and coupling [17]. It is also difficult to fabricate but with a fixed skew can be easier to implement than an optimized Bethe-hole coupler.

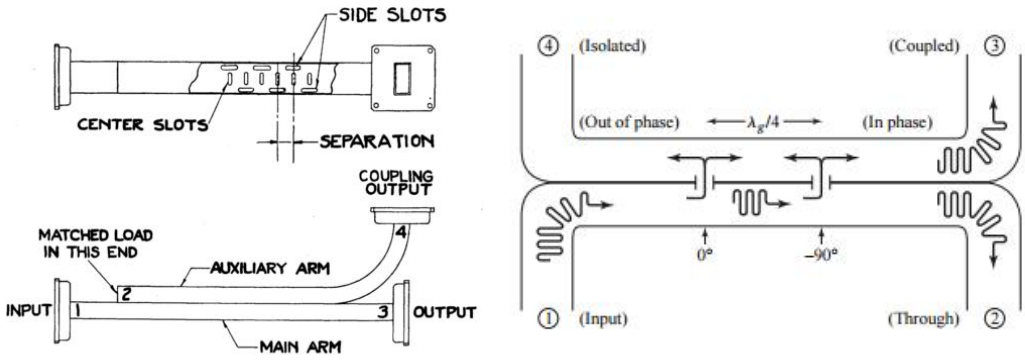

(a)

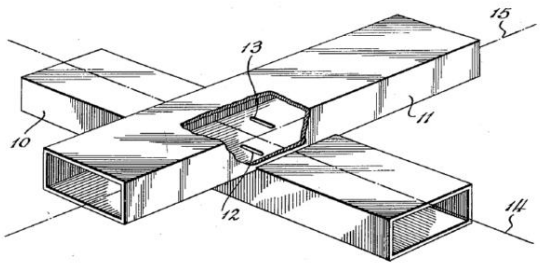

(b)

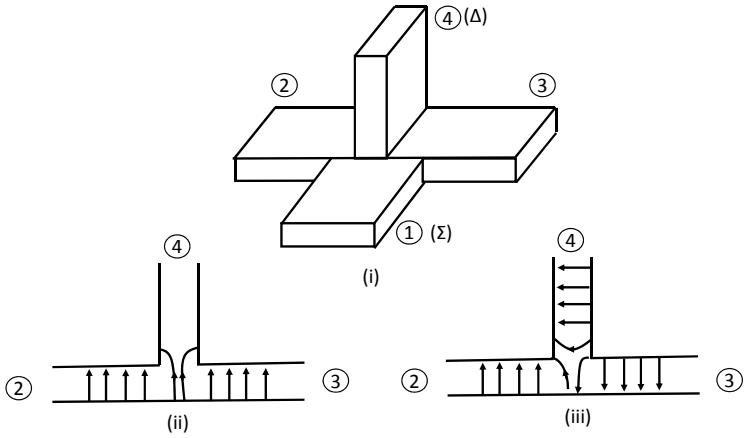

(c)

Figure 4: Examples of directional waveguide couplers (a) Bethe-hole coupler with fourth isolated port sealed [46] and the illustrations of wave generation [44]; (b) Schematic of basic Moreno coupler implemented with two slot apertures [17]; (c) (i) Geometry of a magic T coupler with propagation of waves when (ii) port 1 is the input port and (iii) port 2 is the input port.

Magic T waveguide couplers, designed by W.A. Tyrrell [55], operate using a specific three-dimensional geometry to create high coupling, bandwidth and directivity. As show in Fig. 4c, there are two possible excitation ports, 1 and 4, with their respective field lines represented. When the Σ (port 1) is excited there is uneven symmetry between ports 1 and 4, indicating there will be no coupling between them, instead the power will be split equally and be in phase between ports 2 and 3. When the Δ (port 4) is excited port 1 will decouple and the power will split evenly between ports 2 and 3 but this time with a 180° phase difference. Magic T's are 3 dB couplers that are often used as an alternative to a rat race coupler, an interconnected quarter-wave transmission line coupler.

2.1.2 Coupled-Line Couplers

There are two basic types of coupled-line couplers pictured in Fig.5. The simplest type of coupled-line coupler uses two lines that use edge-side coupling to couple to one another, such as two non-shielded wire next to each other. This simple structure has a low coupling coefficient and bandwidth so Lange couplers and multi-section couplers were developed to optimize its functionality. These geometries are most commonly fabricated using microstrip and coplanar waveguide. Coplanar waveguide is more time consuming to fabricate but can yield to higher isolation than microstrip [57] [16].

The Lange coupler was designed by J. Lange in 1969 [30] and is one of the most commonly used planar coupled-line couplers because of it high coupling coefficient. The coupling coefficient is larger than that of a generic two-line coupled-line coupler because of several very narrow lines (interdigitated striplines) connected in parallel with bond wires as shown in Fig. 5a, obtaining coupling levels of 3 dB. The number of lines and their affects on coupling and directivity have been analyzed [50]. The bond-wire location, pictured in Fig. 5a is essential in order for the coupler to work as it affects phase and helps compensate for unequal odd and even mode velocities.

The total length of this coupler is about $\lambda/4$ with the total width corresponding to $50\,\Omega$ at the center frequency. The width between parallel lines, the number of parallel lines and their odd-mode capacitance all affect the coupling coefficient and directivity (which is low) [11]. This coupler topology is scalable and has been demonstrated to be Q-band, where the frequency scaling is limited by fabrication tolerance [35]. Several attempts have been made to increase bandwidth and directivity [43], [27], and [5], with highest bandwidth obtained by the order of a decade, coupling for 3 dB and loss of 0.25 dB, commercially available from [54], [1] also reports isolation of -24 dB and bandwidth of a little less than a decade.

Both the tapered-line coupler and multi-section coupler are examples of slight geometric alterations to a typical two-line coupled-line coupler. A tapered line coupler, Fig. 5b, is a two line coupled-line coupler where, as the lines separate, the coupling varies. This gradual separation of the lines minimizes the reflections along the line and allows the structure to be high pass and functional at high frequencies [34].The tapered line coupler is often used as a filter because of its minimized reflections [33]. The multi section coupler is used to increase the bandwidth of the common two-line coupled-line coupler by cascading quarter wavelength coupled-line sections with increasing separations, as seen in Fig. 5b. Although the bandwidth increases, the coupling is usually weak and is correlated to the lengths of each section. The tapered lines and multi-section coupled-line couplers are easy to fabricate, however they have low coupling because of fabrication tolerances (require very close proximity similar to two-line coupled-line coupler) and are often too long. All coupled-line couplers are highly affected by fabrication tolerances and phase velocity mismatches which degrade coupling, directivity, and bandwidth.

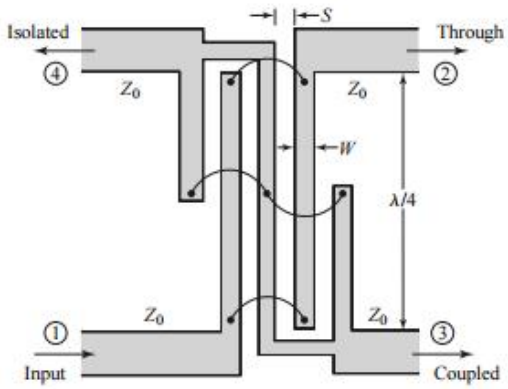

(a)

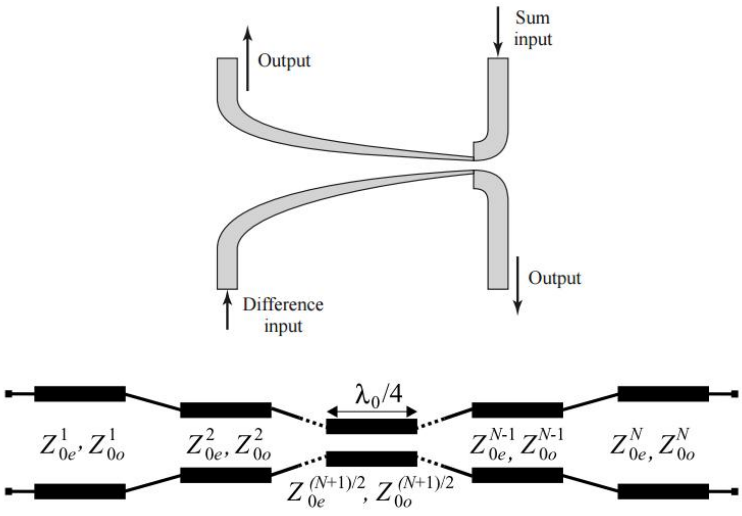

(b)

Figure 5: Examples of coupled-line couplers (a) Basic topology of a Lange coupler with bond-wire placement shown [44]. (b) Schematic of a tapered coupled-line coupler [44] and multi-section coupled-line coupler [36].

2.1.3 Interconnected quarter-wave transmission line couplers

The interconnected quarter-wave transmission line couplers consist of connected transmission line sections and use multiple reflections to achieve coupling and isolation. These designs, shown in Fig. 6, are easily analyzed using odd and even mode analysis [44] and can be fabricated using microstrip, coplanar waveguide, or stripline.

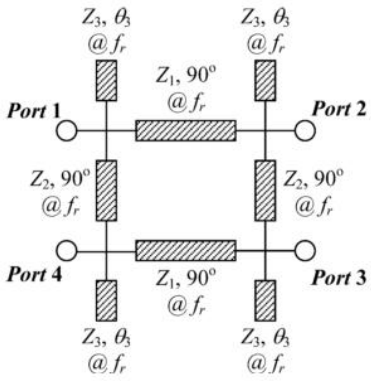

(a)

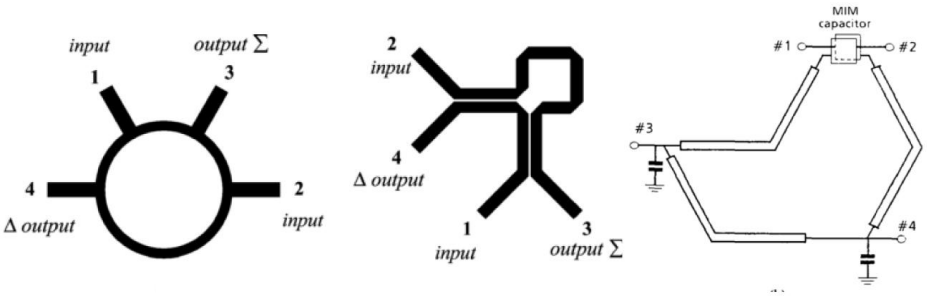

(b)

Figure 6: Examples of edge-side couplers (a) Branch line coupler schematic illustrating the impedance and phase shift correlated to each transmission line segment [51]. (b) Multiple rat-race topologies, [37] for the two on the left, and [21] for the one of the right.

Branch-line couplers are symmetric planar couplers (as shown in Fig. 6a) with a topology that can be easily designed to result in different power division by adjusting the length of the transmission line between each port. For a 3 dB coupler, each individual section is a quarter of a guided wavelength long, which results in a 90° degree phase shift between input and output ports. This coupler is a popular planar coupler because of its high directivity and coupling, and is often used as a power combiner and divider, as well as in analog phase shifters and balances mixers. The difficulty with this coupler is decreasing its size and increasing its bandwidth because

each arm's impedance is designed for a specific center frequency because of the quarter wavelength requirement. Miniaturization, was first tried by fabricating the branch line with microstrip [22] but miniaturized even further with specific geometries or materials [51]. It has also been developed using CPW (coplanar waveguide) and CPS (coplanar strips) [22]. Increasing the bandwidth of the coupler can be done by cascading multiple branch-lines, however this increases loss. There have been couplers designed specifically for broadband applications without degrading the performance of the coupler [53] where a multi-layer design was implemented, achieving a 20 - 30 GHz frequency band.

Visually understanding how a branch-line coupler works is not intuitive, the following is a simple explanation of how power coupling and isolation is achieved. Given a branch-line coupler, such as the one shown in Fig. 7a, where ports 3 and 4 have a Z_0 load and port 2 is shorted to show that; (1) port 1 is matched, (2) power divides equally between ports 3 and 4, (3) the voltage at port 4 lags port 3 by 90°, (4) the voltage at port 3 lags input voltage by 90°, and (5) and there is not voltage at port 2.

First, (1) if port 2 is shorted, ports 1 and 4 see an open reducing the circuit to Fig. 7c, from which the input impedance is calculated to match port 1;

$$Z_{in} = \frac{(Z_0/\sqrt{2})^2}{Z_0/2} = Z_0 \tag{4}$$

Second, (2) ports 3 and 4 present the same impedance, as seen in Fig. 7b, therefore the power is split evenly between the two ports. (3) The voltage at port 4 lags port 3 by 90° because of the quarter wavelength separation. There is no reflection from the line at port 4 because it is terminated in a load Z_0. (4) This simplifies the total current in the system to;

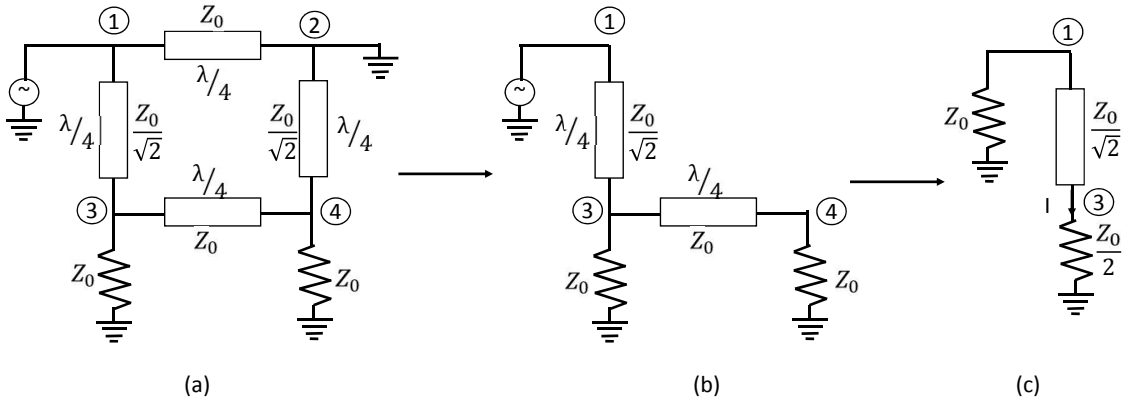

Figure 7: Circuit reduction of a branch-line coupler when port 2 is shorted (a) the original branch-line coupler with transmission line lengths and impedances; (b) simplified when port 2 is shorted and; (c) further simplification where ports 3 and 4 are consolidated.

$$I = -\frac{jV_1}{Z_0}\sqrt{2}\ , \tag{5}$$

where the current lags the input voltage by 90°;

$$V_3 = I\frac{Z_0}{2} = -\frac{V_1}{\sqrt{2}}\ , \tag{6}$$

indicating the voltage at port 3 lags voltage at port 1 by 90°, only when the impedance where Z_0 is real. (5) The last property to show is there is no current at port 2, so that with can be shorted without impacting the circuit. Looking at Fig.7a, V_4 lags V_3 by 90° which lags V_1 by another 90°, therefore V_4 lags V_1 by 180° with a magnitude of $\sqrt{2}V_1$ (half of the power). The magnitude of the current at port 2 will be equal but opposite in phase because the $Z_0/\sqrt{2}$ impedance, where ports 2 and 4, compensates for the $\sqrt{2}$ voltage magnitude difference. From this investigation port 2 is determined to be isolated and ports 3 and 4 are coupled with a coefficient of 3 dB.

Rat race (ring hybrid) couplers are lossless, matched and reciprocal couplers that have a 180° degree phase shift. They are popular planar couplers as they can be easily

fabricated using microstrip or stripline. By using different lengths of transmission line the coupling coefficient can easily be controlled with very little loss. The lines are designed to be a matched to each port, usually with a total length of one and a half wavelengths. This results in high coupling, and good directivity. The bandwidth is usually between 20 - 25% but can be increased by adjusting the lengths of each section [22].

2.1.4 Broadside Couplers

Broad-side coupling is not a commonly used coupling mechanism, but there have been designs that take advantage of the capacitive like structure. It can be made with both coplanar waveguide and microstrip and often utilizes a four layer substrate, as shown in Fig. 8 with an upper and lower ground [48]. Broadside couplers are often fabricated to be used in tandem with another RF structures, such as high bandwidth filters [32].

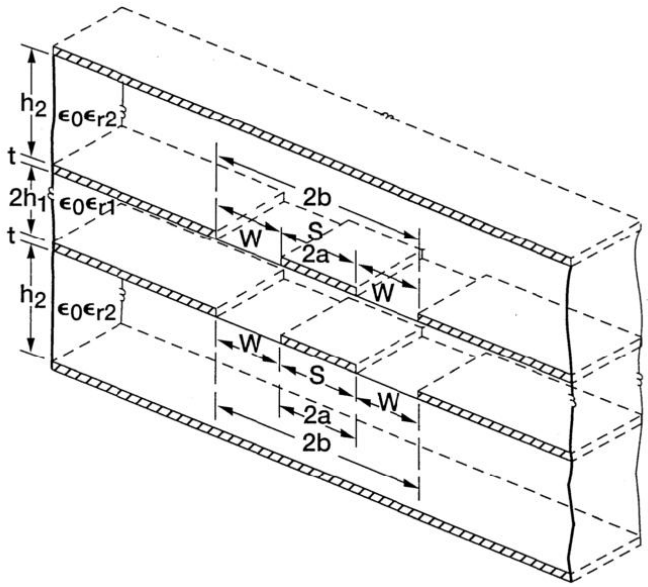

Figure 8: An illustration of a basic coplanar waveguide broad-side coupler [48]. A single coplanar waveguide with some width S and separation from ground W is separated by some h_1 above another coplanar waveguide. This system shows a symmetric system with ground above and below the coupler.

With variations in structure (e.g. asymmetric coplanar waveguides, or top and bottom ground removed), broad-side couplers can achieve a high coupling coefficient (3 dB) but suffer from a very narrow bandwidth [6]. The highest isolation, coupling, and bandwidth shown has been below 20 dB, 3 dB, and 0.3 decades respectively [52]. A higher bandwidth can be achieved by using a multisection (coupled-line coupler) coupler with a broad-side junction [26]. This hybrid between edge-side and broad-side coupling is the basis for the coupler described in this thesis.

2.2 Couplers in Literature

As the previous chapter described, the coupler discussed in this thesis was designed with the intent of being implemented in a compact, planar, high frequency (between UHF and EHF) environment. The coupler is required to have a high coupling coefficient and high directivity. Table 2 shows a brief review of a few papers that have adjusted coupler topologies to; miniaturize, increase operating frequency, or optimize s-parameter characteristics. A short description of each coupler and their characteristics oulined in that paper is given. None of the couplers satisfy all of the requirements but give a few examples of what coupler designs have incorporated some of the above characteristics.

Frequency can be shifted by adjusting the lengths of the coupled transmission lines and changing the materials used. However, the basic couplers have a maximum frequency depending on fabrication tolerances, going to higher frequencies requires designing hybrids and miniaturizing the couplers in different way. Although not listed in the Table 2, previous ways to miniaturize couplers included adding lumped components to achieve the same impedance of a transmission line without incorporating the whole length, meandering lines, and fractal-line sections [15]. These are viable options but rely heavily on fabrication tolerances (fractal lines and meandering lines) and suffer from implementation issues (lumped elements).

Table 2: A Brief Review of Miniaturized, Multilayer or High Frequency Couplers in Literature

Reference	**Description**	**Characteristics**
[7]	- multilayer using $\lambda/4$ lengths - A combination of Lange and ring hybrid - Lange coupler uses broad-side coupling to miniaturize and remove bond wires	- 25 - 35 GHz frequency range - high bandwidth but low isolation and directivity - 20 dB S_{11}, 15 dB S_{41}, 5 dB S_{21} and S_{31}
[19]	- miniaturized rat race - uses compact resonant micro strip cell which uses slow wave effects	- 1 - 10 GHz - high isolation between ports - 23 dB S_{11}, 25 dB S_{41}, 5 dB S_{21} and S_{31}
[24]	- miniaturized branch-line and rat race couplers - designed to created two frequencies of operation - 21 % of conventional circuit area	- multiband operation (2.5 and 5 GHz) - 25 dB S_{11} and S_{41}, 5 dB S_{21}, 2 dB S_{31} at 2.5 GHz (branch-line) - 20 dB S_{11} and S_{41}, 1 dB S_{21} , 9 dB S_{31} at 5 GHz (branch-line) - 22 dB S_{11} and S_{41}, 1 dB S_{21} , 6 dB S_{31} at 2.5 GHz (rate-race) - 30 dB S_{11} and S_{41}, 2 dB S_{21} , 5 dB S_{31} at 5 GHz (rat-race)
[40]	- multilayer coupler based on lange coupler - uses broadband coupling - symmetric meander configuration with 15 μm separation	- 10 - 17.5 GHz - 15 dB S_{11}, 20 dB S_{41}, 5 dB S_{21} and S_{31}
[37]	- uses basic hybrid rat race coupler - the input and output ports are on different layers	- 24 GHz coupler - 15 dB S_{11}, 3 dB S_{31} - 30% reduction of rat race area of same frequency -Tolerances for fabrication misalignments high
[42]	- micromachined coupler that can be easily integrated with RF systems - elevated structure using different air/dielectric combinations -impedance is limited by width and separation of the coupled lines	- broadband (15 - 45 GHz) -11 dB S_{11}, 3 dB S_{21}, 15 dB S_{31}, and 20 dB S_{41}

As multi layer fabrication is heavily involved in circuitry, many of the references below have tried taking advantage by using broad-side coupling as in [7]. Although broad-side couplers are not classical couplers, using it in tandem with edge-side coupling can be useful. Broadside coupling alone is more often used for probes because of its similarity to a capacitor. For example, [23] analyzed the theory behind multilayer planar couplers comparing edge and broad-side coupling as well as the physical parameters to theoretically design 1 dB, 6 dB, and 10 dB couplers while [28] has theorized optimal dielectric thickness and ratios. Different materials have been experimented with to try miniaturize and optimize the designs even further [4] [47]. There has been some designs using multiple lines in multiple layers, such as [18]. This design used three lines to create a coupler at 2.5 GHZ. However, because of its asymmetric topology it requires compensating capacitances.

The coupler discussed in this thesis will look at scaling in frequency, no additional components (compensating impedances), and achieve good high coupling and directivity using a symmetric, multi-layer design. The coupler is designed so that only the length of the coupler is changed to alter the operation frequency. The impedance of the coupled-line section of the coupler is designed to match a 50 Ω sma cable without compensating capacitors. High coupling and directivity are directly correlated to the dimensions of the coupler, the ratios between layers, and it symmetry.

Chapter III

COUPLED-LINE THEORY

In the previous chapter, an overview of various types of couplers is presented. This chapter will focus on the theory behind two-line couplers, including edge and broad-side coupling. A brief discussion on the effects of combining broad-side and edge coupling in a multilayer system is also presented.

3.1 Edge Coupling

Coupling occurs between two transmission lines when their electromagnetic fields are not independent due to proximity. There are two distinct coupling mechanisms: electric and magnetic. This can be understood by considering the simple example of two electrically short sections of line, as illustrated in Figure 9. When line 1 is open-circuited and connected to a voltage source $v_s(t)$, a voltage will appear across the load on line 2 which is also open-circuited. This is due to electric field coupling and can be represented by a capacitance between the two lines. On the other hand, when line 1 is terminated with some load allowing current to flow, and line 2 is terminated so that it can also support current flow, coupling occurs through electromagnetic induction given by Faraday's law. This can be represented by a mutual inductance between the two lines. Of course, the situation is more complicated when the lines are long enough to support voltage and current waves, as will be shown later in this chapter.

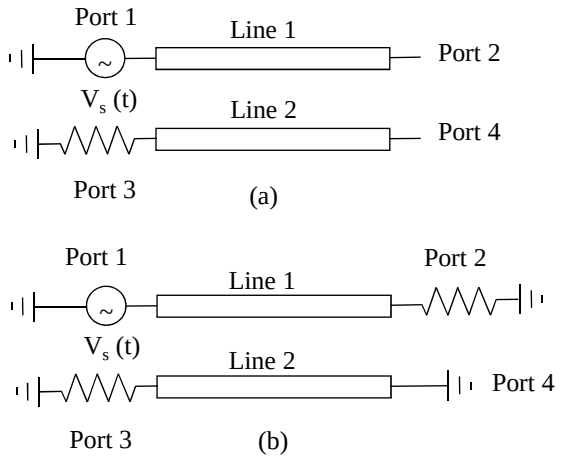

Figure 9: A simple illustration of a two line system and its (a) electric and (b) magnetic field coupling circuit setup.

For uniform transmission lines, such as a coaxial cable and a two-wire line, the field is TEM, i.e. the electric and magnetic fields are limited to the plane transverse to the direction of propagation. Only the TEM mode will propagate over a broad frequency range, essentially from DC to a frequency that depends on the geometry (physical size and dielectrics) of the line when other modes can exist. If the dielectric of a guiding structure is not uniform, such as in microstrip lines, a small component of the field exists in the propagation direction, resulting in a quasi-TEM mode. This mode can be mathematically described using the same formulas as for a TEM case, but with an effective dielectric constant and effective propagation constant which depend on the line geometry and frequency. In the case of two coupled microstrip lines, the electric and magnetic fields can have two distinct distributions at any transverse cross-section, illustrated in Fig. 10. As waves propagate along the lines, the polarity of the voltages will be either equal or opposite, resulting in even and odd modes, respectively [11].

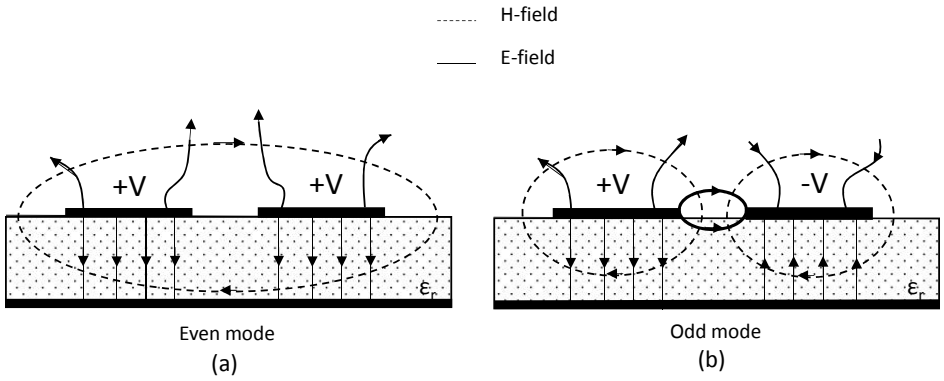

Figure 10: Sketch of magnetic and electric field lines of two coupled lines for (a) even and (b) odd mode fields. The density of fields resulting from the different permittivities (ϵ_0 and ϵ_r) are visualized with the different number of lines. The bottom electrode is assumed to be at zero potential.

Figure 11 depicts the top view (layout) of two microstrip lines that come close to each other along a section that has a certain length L. The ports of this 4-port network are as follows: P1 is the input, P2 the through, P3 the coupled, and P4 the isolated port.

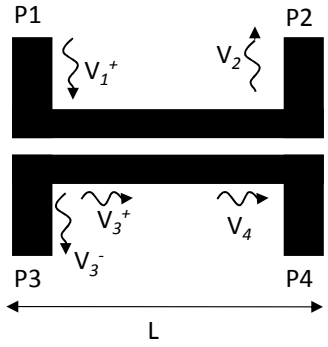

Figure 11: The layout of a four port microstrip coupler with a basic edge-side coupler orientation P1 is the input port, P2 is the through port, P3 is the coupled port and P4 is the isolated ports. The characteristic S-parameters outlined in Table **??** are calculated based on the propagating voltages.

When port 1 is excited with an incident wave, V_1^+, as soon as the wave reaches the coupled line section it will couple capacitively to port 3 resulting in waves V_3^- and V_3^+. The coupled wave will propagate along the coupled line section until it reaches the end of it with some phase delay. The above assumes none of the wave was reflected back toward port 1 which is not necessarily true because the second line in close proximity to the first line alters the impedance at port 1. This can be eliminated by adjusting the geometry of both the port and coupled line section to obtain match at port. By adjusting length, width, and separation the voltage coupled to port 3 and propagated through to ports 2 and 4 can be controlled and used to define the characteristic S-parameters of the system, as shown in the Table 3 below.

Table 3: S-parameter definitions and their corresponding ideal values

S-Parameter	**Physical Meaning**	**Ideal Value**
$-20\log\lvert S_{11}\rvert$	return loss - quality of match at port 1	∞ dB
$-20\log\lvert S_{21}\rvert$	through - amount of voltage transfered to port 2	0 dB
$-20\log\lvert S_{31}\rvert$	coupling factor - fraction of power coupled to port 3	C dB
$-20\log\lvert S_{41}\rvert$	isolation - measure of the amount of power that is at port 4	∞ dB

It can be shown that a matched, reciprocal, lossless 4-port has to have a port isolated, and that because of symmetry, the ports are 90-degrees out of phase. The facts that port 1 is matched, port 4 isolated and ports 3 and 4 are in quadrature, will not change with the length of the coupled line section length. The only thing that changes is the coupling coefficient. (Note that this is quite different than in the case of the branch-line coupler, which depends on phase-dependent additions and cancellations at the ports, resulting in frequency dependence.) However, any changes in the separation, thickness of dielectric or copper, the dielectric constant, width of coupled lines, etc will affect the S-parameters, some such relations can be found in [2] and [12].

The following sections will look at the capacitive and inductive coupling separately

for a short and long coupled-line section. By understanding these components one can both evaluate and manipulate the geometry of the coupler to obtain optimal S-parameters.

3.1.1 Electrically-Short Coupled-line Section

Consider an edge-side coupler with a wavelength much longer than the coupled-line length and an incident time harmonic wave with RMS value V_1 at port 1, shown in Fig. 12. We can assume that V_1 and I_1 do not change along the line. For the moment, we also assume that the coupled current and voltage on line 2 do not affect the current and voltage on the source line 1. Fig. 12 illustrates the capacitive coupling components when both lines are resistively terminated in Z_0 at both ends.

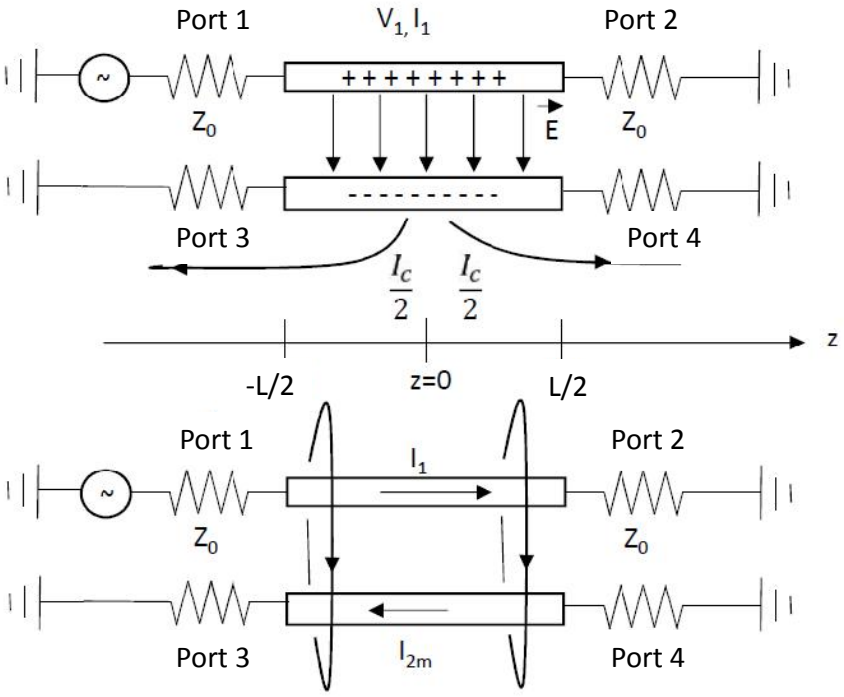

Figure 12: Four port-coupler of some length L terminated with Z_0 at all ports. The top four-port illustrates capacitive coupling while the bottom diagram describes inductive coupling.

The mutual capacitance can be found by investigating the current induced on the

second line. Given a voltage incident on port 1, there will be a resulting voltage on line 2 and a current that flows toward the terminating loads at ports 3 and 4. The current I_c leads the voltage by 90°, where current at port 3 is flowing in the $+z$ direction and at port 4 the current is flowing in the $-z$ direction. The symmetry of the system gives a reference point for the current so that a general transmission line equation can be integrated over the distance of the coupled line to form:

$$\frac{\mathrm{d}I_2}{\mathrm{d}z} = I_2' = -j\omega C_m' V_1 \ , \tag{7}$$

$$\tag{8}$$

$$\int_0^z \frac{\mathrm{d}I_2}{\mathrm{d}z} = \int_0^z -j\omega C_m' V_1 \ , \tag{9}$$

$$\tag{10}$$

$$I_{c2} = -j\omega C_m' V_1 z \ , \tag{11}$$

The coupled line section can be viewed as a parallel connection of small capacitors (which add up to C_m), which means that the current is a function of a distance along the line, where z from Eq. (11) can be replaced by $L/2$ for the example shown in Fig. 12. The mutual capacitance has to be negative because of the current's phase.

The mutual inductance can be found in a similar manner where the source at port 1 is a current source that induces a current, on line 2, that opposes the flux by Faraday's law. There is now a voltage on port 3 and an opposite and equal voltage on port 4. The symmetry provides a reference point which can be used to integrate the transmission line equation to obtain (the same process was used above for the capactive coupling):

$$V_{c2} = -j\omega L_m I_1 z \tag{12}$$

Similar to the capacitive case, the voltage is a function of distance along the coupled line. The mutual inductance is positive because the induced voltage lags I_1. Combining the capacitive and inductive components from Eq. (11) and (12) shows

that the voltages add in phase at port 3 (coupled port) and out of in phase at port 4 (isolated port). The isolated port is completely isolated if the impedance satisfies;

$$Z_0^2 = -\frac{L_m}{C_m} \tag{13}$$

The short coupler gives a basis for characterizing a transmission line coupler. It shows how capacitive and inductive coupling create currents and voltages that add and cancel at ports 3 and 4, respectively. However, couplers will more likely be comparable or longer than the operating wavelength. This changes the investigation because now the self inductance and capacitance will have to be considered in characterizing the voltage and current coupling.

3.1.2 Electrically-long Coupled-line Section

When the coupled-line length is larger than the wavelength the self impedances of the line are no longer negligible. This means that the transmission-line equations can be written as:

$$\begin{pmatrix} I_1' \\ I_2' \end{pmatrix} = -j\omega \begin{pmatrix} C_s & C_m \\ C_m & C_s \end{pmatrix} \begin{pmatrix} V_1 \\ V_2 \end{pmatrix} \tag{14}$$

$$\begin{pmatrix} V_1' \\ V_2' \end{pmatrix} = -j\omega \begin{pmatrix} L_S & L_m \\ L_m & L_S \end{pmatrix} \begin{pmatrix} I_1 \\ I_2 \end{pmatrix} \tag{15}$$

where the primes indicate the derivate of the current or voltage, the capacitances are all distributed per unit length (F/m), and the inductances are also per unit length (H/m). Now the solutions to these equations can be found in terms of the odd and even modes as follows:

$$V_e = \begin{pmatrix} 1 \\ 1 \end{pmatrix} e^{(\mp\beta_e z)} \ , \tag{16}$$

where $\beta_e = \sqrt{(L_S + L_m)(C_S + C_m)}$ and $Z_e = \sqrt{\frac{L_S + L_m}{C_S + C_m}}$ and,

$$V_o = \begin{pmatrix} 1 \\ -1 \end{pmatrix} e^{(\mp\beta_o z)} \ , \tag{17}$$

where $\beta_o = \sqrt{(L_S - L_m)(C_S - C_m)}$ and $Z_o = \sqrt{\frac{L_S - L_m}{C_S - C_m}}$.

This suggests that the coupler can be separated into two problems corresponding to the even and odd modes as long as symmetry is preserved. The simplest coupler is a quarter-wave coupler. When even and odd mode propagation constants are equalized, the S-parameters for an ideal coupler can be characterized in terms of the reflection and transmission coefficients.

3.1.3 Even and Odd Mode Impedances

Using the even and odd mode fields shown in Fig. 10 one can draw an equivalent capacitances of the even and odd modes as shown in Fig. 13. The even and odd mode capacitance can be written as $C_e = C_p + C_f + C'_f$ and $C_o = C_p + C_f + C_{ga} + C_{gd}$ where C_f, C'_f, C_{ga} and C_{gd} are the various fringing capacitances of the systems.

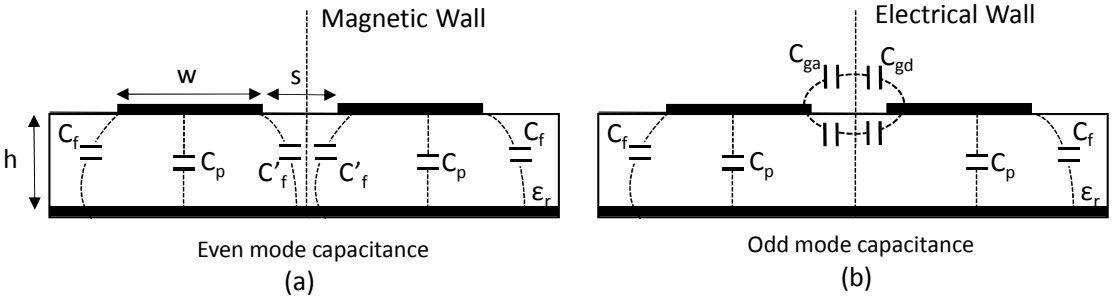

Figure 13: The even and odd mode capacitances decomposed into their individual components, where C_f, C'_f, C_{ga} and C_{gd} are the fringing capacitances. Many references use this model, e.g. [11].

All of these capacitances can be expressed in terms of each other and the ratio

between the width of the microstrips (w), the height of the dielectric (h), and the permittivity of the system. The following equations which are available in multiple works including, [12] and [11] show how by using the total odd and even mode capacitance components one can calculate the even and odd mode impedances.

$$C_p = \epsilon_o \epsilon_r \frac{W}{h} \ , \tag{18}$$

$$2C_f = \frac{\sqrt{\epsilon_{eff}}}{cZ_0} - C_p \ , \tag{19}$$

$$C'_f = \frac{C_f}{1 + A(h/s)\tanh(8s/h)} \ , \tag{20}$$

where $A = \exp(-0.1\exp(2.33 - 2.53W/h))$,

$$C_g a = \epsilon_0 \frac{K(k')}{K(k)} \ , \tag{21}$$

where $k = \frac{S/h}{S/h+2W/h}$, $k' = \sqrt{(1-k^2)}$, and

$$\frac{K(k')}{K(k)} = \begin{cases} \frac{1}{\pi}\ln\left[2\frac{1+\sqrt{k'}}{1-\sqrt{k'}}\right] & 0 \le k^2 \le 0.5 \\ \ln\left[2\frac{1+\sqrt{k'}}{1-\sqrt{k'}}\right] & 0 \le k^2 \le 0.5 \end{cases} \tag{22}$$

$$C_g d = \frac{\epsilon_0 \epsilon_r}{\pi} \ln\left[\coth\left(\frac{\pi}{4}\frac{S}{h}\right)\right] + 0.65 C_f \left[\frac{0.02}{S/h}\sqrt{(\epsilon_r)} + 1 - \epsilon_r^{-2}\right] \tag{23}$$

The linear combinations of these equations for the total even and odd mode capacitances can be used to find the even and odd mode impedances of the system as follows;

$$Z_{0e} = \frac{1}{c\sqrt{C_e C_{e1}}} \ , \tag{24}$$

$$Z_{0o} = \frac{1}{c\sqrt{C_o C_{o1}}} \tag{25}$$

where c is the velocity in air and $\epsilon_{effe} = \frac{C_e}{C_{e1}}$ and $\epsilon_{effo} = \frac{C_o}{C_{o1}}$. These calculations were done assuming the lines are of finite thickness. Extra steps must be taken if copper line thickness is taken into account. These calculated results are comparable to the Bryant and Weiss [56] method.

3.2 Broad-side Coupling

As multilayer fabrication techniques have evolved, using broad side coupling has become more feasible. The analysis for edge-side and broad-side coupling are similar, so a summary of the results are presented in this section. Typically, broad-side coupling is considered when both lines are strip-lines or coplanar waveguide. A two line system with a broad-side cross-section is shown in Fig.14. The even and odd modes are created by two orthogonal TEM modes propagating along the lines, when the voltages and currents are equal in amplitude and either in or out of phase [9]. All other voltages and currents in the system can be expressed as linear combinations of these two modes.

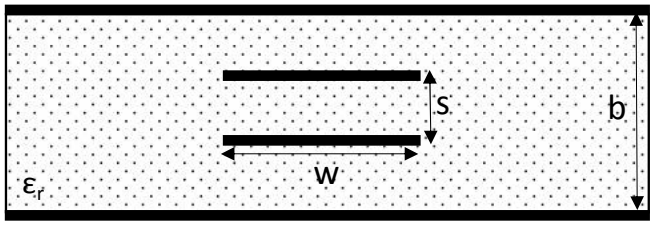

Figure 14: Cross-section of two-line, stripline, broad-side coupling system. The evaluation techniques are similar to those used for edge-side coupling.

There are many methods for calculating the even and odd mode impedances, one of the ways uses the Schwarz Christoffel conformal mapping [8]. Analogous to the even and odd mode impedances given previously for edge-side coupling, the impedances for a system shown in Fig. 14 are:

$$Z_{0e} = \frac{188.3}{\sqrt{\epsilon_r}} \frac{K(k')}{K(k)} \ , \tag{26}$$

$$Z_{0o} = \frac{296.1s}{b\sqrt{\epsilon_r}\tanh^{-1}(k)} \tag{27}$$

where $\frac{K(k')}{K(k)}$ is given in (22).

The above equations show the impedances for a two line system with pure TEM-modes, however most systems will have both a quasi-TEM and TEM wave propagating along the two lines. This analysis is much more complex, however as discussed above all of the voltages and currents can be expressed as linear combinations of the even and odd modes and for this reason we assume that the above is a reasonable approximation for a microstrip line multilayer system.

3.3 Combined Broadside and Edge Coupling

Notice from the above two sections that both edge-side and broad-side coupling are affected by width, separation, and dielectric thickness and permittivity. However, both designs are limited by fabrication tolerances and separately cannot achieve the optimal S-parameters for the application discussed in this thesis. The question becomes what happens when both broad-side and edge-side coupling are combined into the same structure. From the previous investigation, one can determine that for edge coupling the odd-mode velocity is larger than the even-mode velocity. This is because the odd-mode electric field is primarily contained in the air while the even-mode electric field is more constrained to the dielectric region, as shown in Fig. 10. Conversely, the even-mode velocity is larger than the odd-mode velocity for broad-side coupling because most of the electric field is constrained in the region between the transmission lines [10].

There are many possible geometries for devices that use both types of coupling, most notably, [23] and [18]discussed in the previous chapter. However, neither of

these are symmetric, so this section will look at the effects of a symmetric, multilayer topology where the interconnects between coupling lines matters.

Fig. 15 shows the S-parameters of four lines where the two lines in the second layer are open circuited (not connected to each other or the top layer). The low coupling, low directivity and high return loss do not meet the specification required. In the simulation tool, separation between the two lines, the width of the lines, and the length were all adjusted to try and optimize the coupler to the required S-parameter values. The separation, and width of the lines was not the same on both layers and both dimensions ranged from 0.2 to 5 mm, while the length ranged from 5 to 50 mm for a 1 GHz coupler. No combinations of these parameters matched the even and odd mode impedances. Similarly, if the lines are connected to the ones directly above and below each other the impedances are not compensated for with similar characteristics as shown in Fig. 15.

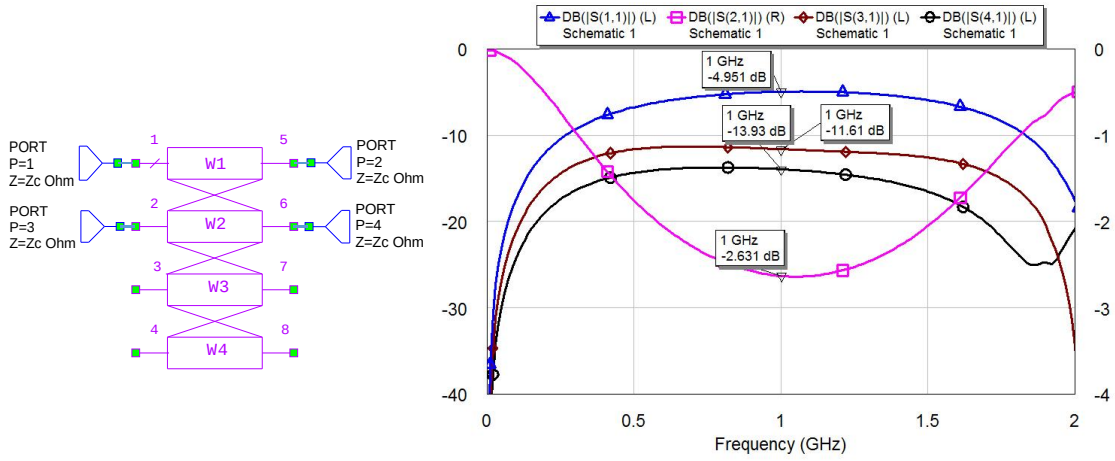

Figure 15: (a) The AWR layout for a four-line multilayer coupler where the lines on separate layers are not connected. (b) S-parameters corresponding to this topology. S_{11}, S_{31}, and S_{41} are on the left axis while S_{21} is on the right axis. This geometry results in very poor matching at port 1, low coupling, and low directivity.

With a single section of coupled line a high level of coupling cannot be achieved without bringing the two coupled lines very close together. By using several coupling lines that have a lower coupling coefficient and connecting them, such as the multi-section or Lange coupler, higher coupling can be achieved. However, once these extra lines are added, very similar to the Lange coupler, the location of connections between the lines, or analogously the interdigitating striplines, is necessary for a functioning design. The best connection for a four-line coupler is between diagonally opposite lines. Unlike the other connections, such as the one shown in Fig. 15 this orientation can help coupling and directivity while minimizing loss. The following section will focus on illustrating the capabilities of symmetric, multilayer, layouts utilizing a diagonal connection.

Chapter IV

SIMULATION AND MEASUREMENT

The coupler presented in this chapter is based on previous work on a four-line coupler described in [39], but it is implemented at a 10 times higher frequency. The coupler geometry is shown in Fig. 16, where the top-layer and bottom-layer microstrip lines are connected diagonally. The coupler uses multiple layers to increase the coupling, unlike other hybrid couplers, such as the Lange and multi-section couplers. The high bandwidth and low loss consistent with coupled-line couplers is preserved with the benefit of reduced surface area. This coupler design also increases the coupling coefficient and directivity compared to a general coupled-line coupler. This chapter will discuss the simulations and measurements of the optimized multilayer coupler.

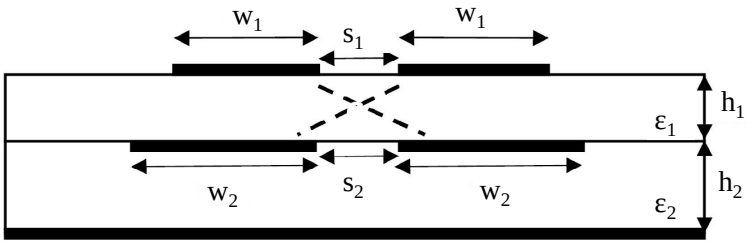

Figure 16: A transverse cross-section of a three-layer topology. The dashed lines indicate which of the coupled lines are connected with vias. The dielectric heights between the ground the coupled lines are not the same. The widths w_1 and w_2 as well as the separations s_1 and s_2 are variables used for optimization.

4.1 Procedure Background

This section briefly describes the design, simulation tools, fabrication specifications, and calibration method used to obtain the measured results.

4.1.1 Design Overview

The coupler described in this thesis proposes to combine edge-side and broad-side coupling with four transmission lines. Fig. 16 shows the four transmission lines, where top layer and bottom layer coupled lines have widths w_1 and w_2 (same on individual layers to keep symmetry) respectively and separation between the coupled lines of s_1 and s_2 respectively. The heights h_1 and h_2 of the dielectric are not equal because the ratio between the two affects the coupler's characteristics while the permittivity of the dielectric is the same for both layers to minimize the variations in even and odd-mode field density. With the lines connected diagonally, the geometry is expected to balance even-mode and odd-mode characteristics. Ideally the vias used to connect the layers would not introduce any parasitic reactances and would be distributed along the length of the entire structure. However, to keep symmetry and satisfy fabrication limitations, there are only four vias on either end of the coupled lines.

The specific implementation of the transmission lines connected to four ports affect the coupler components. Remember from the theory chapter, to get optimal S_{11} the coupler has to be matched to port 1. This means that the impedance of ports are designed to match the input impedances of the coupled-line section. Ideally the port could be designed around the coupled-line section, however because of measurement restrictions (size of SMA connectors and impedance of the coaxial cables), the coupler had to optimize both ports and coupled-line sections.

4.1.2 Simulation Tools

Three simulation tools were used to design and analyze the coupler: NI/AWR Microwave Office, NI/AWR AXIEM [25], and CST [49]. AWR is a straightforward, two-dimensional simulation tool that uses method of moments (MOM) to evaluate the model. This tool provided a time-efficient method to evaluate the trends of varying dimensions from Fig. 16. AXIEM is an addition of AWR which also uses MOM

but models in 2.5 dimensions. Although there is no optimization, it was a helpful middle step from converting the 2-D model into a 3-D realization. CST is a three dimensional tool that uses a Integral Equation solver (IES), which is also a MOM simulator. This final tool was used to fine-tune the model designed in AWR, it optimized the S-parameters and took fabrication tolerances into consideration.

4.1.3 Fabrication Specifications

The company used to fabricate the couplers, OSH Park [41], has a few fabrication tolerances. The layout used was a four-layer board with a dielectric permittivity of 3.66 and dimensions outline in Table 4. The two top copper layers (T_1 and T_2) are used for the coupling line while the third layer (T_2) is used as a ground and the four copper layer (T_1) was removed completely for the first generation coupler.

Table 4: Substrate characteristics valid for 1 GHz as well as fabrication limitations for OSH Park

Symbol	**Property**	**Value**
ϵ_r	dielectric permittivity	3.66
σ	copper conductivity	5.7e9 S/m
h_1	dielectric thickness from Fig. 16	0.17 mm
h_2	dielectric thickness from Fig. 16	1.17 mm
$\tan\sigma$	loss tangent of dielectric	0.002
t_1	outer layer conductor thickness	0.035 mm
t_2	two middle layer conductor thickness	0.017 mm
Z_0	characteristic impedance	50 Ω
w	minimal trace and spacing	0.127 mm
v	minimal via	0.254/,mm

Initially the coupler was designed with no fabrication specifications and tuned between 1 and 5 GHz. Theoretically this is not the limit of the designs scalability,

however the frequency for the fabricated couplers is bound to this range because of measurement and limitations provided by OSH Park . However, simple adjustments in dielectric permittivity and thickness can scale the center frequency to beyond the range. Before fabrication limitations were implemented onto the design a few observations made with an AWR simulation should be noted:

- When the thickness of the copper is the same on all layers, from quick AWR simulations, a good dielectric thicknesses is given to be: $h_1 / h_2 = 1/4$ from Fig. 16. This was also shown in [39].

- The top and bottom lines should not overlap completely and can have different widths, separations, or both. This is done to achieve a balance between the even-mode and odd-mode phases and impedances present in broad-side and edge-side coupling.

- Similar to planar two-line couplers as discussed in the previous chapter, the separation does not have an lower limit but does have an upper limit. However, the multilayer couplers are less sensitive to the separation compared to the sensitivity of the two-line coupler.

A 1:4 ratio for the dielectric thicknesses, as stated to be optimal by the first observation, cannot be implemented with the fabrication process available. The 1:4 ratio is appropriate because, although the dielectric has approximately a $1:7$ ratio the copper thicknesses, listed in Table 4, have a $1:2$ ratio so the copper lines are closer but the embedded coupler lines are thinner. This uneven copper thickness helps adjust for the larger dielectric ratio. The second and third observations are limited only by the fabrication tolerances which were 0.127 mm spacings and 0.254 mm diameter vias.

4.1.4 Calibration

Measurements were taken with a N 5224A Vector Network Analyzer using a SOLT coaxial cable. This calibration was done at the end of the coaxial cables and was not done on the substrate, which explains mismatches at higher frequency. Other methods of calibration are discussed in future work.

4.2 Coupler Design

The first design used AWR and CST to analyze its characteristics. This design tried to keep a similar layout as previous work and used only three of the four available layers in the fabrication process.

4.2.1 Simulation

The three-layer, four line coupler was first simulated with the 2D simulation tool, AWR. The model only took the coupled lines into account, Fig. 17, disregarding vias and extra transmission lines, such as ports, and their corresponding impedances. The AWR model, PC4CLIN, can model several edge-side or broad-side coupling microstrip sections [25].

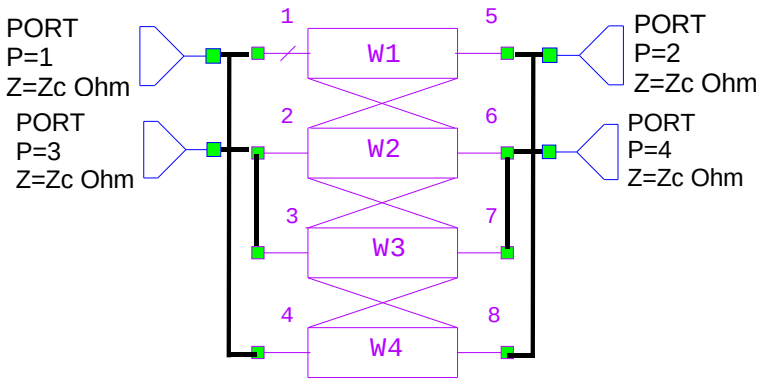

Figure 17: The simplest simulation in AWR for a three-layer, four-port coupler where the four lines are connected in diagonal. No additional transmission line or vias was included in the model.

This AWR design was optimized by tuning the width of the coupled lines in each layer, the separation between the edge-side coupled lines on each layer, and the length. The lower limit for width and separation was 0.2 mm with no upper limit, with no limit for the length. Parameters in Table 6 are such that the width or separation are not increased because the S-parameters deviate too much from the optimal S-parameters. Below is a table that illustrates how changing these parameters affects each s-parameter, the bandwidth (BW), and the center frequency (f_c) of the system. s_1 and s_2 are the separation, w_1 and w_2 are the width for the top and bottom lines respectively, illustrated in Fig. 16, and L is the length of the coupled-line section. The S_{11}, S_{21}, S_{31}, and S_{41} in Table 5 are abbreviations for the definitions outline in Table 3 in the theory chapter.

Table 5: Affects of dimensions adjustments on S-parameters. Dimensions are in mm and S-parameters are in dB and x's indicate the parameter has not changed from the initial value.

S1	**S2**	**W1**	**W2**	**L**	$\mathbf{S_{11}}$	$\mathbf{S_{21}}$	$\mathbf{S_{31}}$	$\mathbf{S_{41}}$	**BW**	$\mathbf{F_c}$
0.5	0.5	0.5	0.5	45	-21.5	-5.141	-1.886	-18.34	~ 1 GHz	0.95GHz
0.25	0.25	x	x	x	-22.82	-5.496	-1.694	-19.17	~ 1.1 GHz	0.95GHz
1.5	1.5	x	x	x	-18.16	-4.491	-2.381	-16.1	~ 1 GHz	0.95GHz
x	x	0.25	0.25	x	-28.21	-4.289	-2.256	-29.82	~ 0.9 GHz	0.95GHz
x	x	1.5	1.5	x	-11.11	-5.369	-3.122	-9.085	~ 1.1 GHz	0.95GHz
0.25	1.5	x	x	x	-30.17	-2.44	-4.003	-28.6	$\sim$0.5GHz	0.95GHz
1.5	0.25	x	x	x	-31.87	-2.656	-3.699	-32.22	~ 1 GHz	0.95GHz
x	x	0.25	1.5	x	-13.81	-3.14	-3.879	-14.6	~ 0.5 GHz	0.95GHz
x	x	1.5	0.25	x	-15.37	-3.37	-3.443	-15.3	~ 0.5 GHz	0.95GHz
x	x	x	x	30	-21.1	-5.164	-1.864	-18.14	~ 1 GHz	1.4GHz
x	x	x	x	65	-21.25	-5.167	-1.88	-18.2	~ 0.75 GHz	0.65GHz

Changing the separations and widths of the lines also changes the impedances of the coupler. A well matched system will increase coupling, isolation, while maintaining high return loss. The length only affects the center frequency and the bandwidth, the separation primarily changes coupling and bandwidth, while the width influences all of the S-parameters. The table also indicates S-parameters could benefit from a design that uses unequal separation and widths on the two layers.

Fig. 18 shows the optimized S-parameters from this initial simplistic simulation. S_{11} and S_{41} are below -30 dB while S_{21} and S_{31} are at -3dB with a center frequency of 1 GHz.

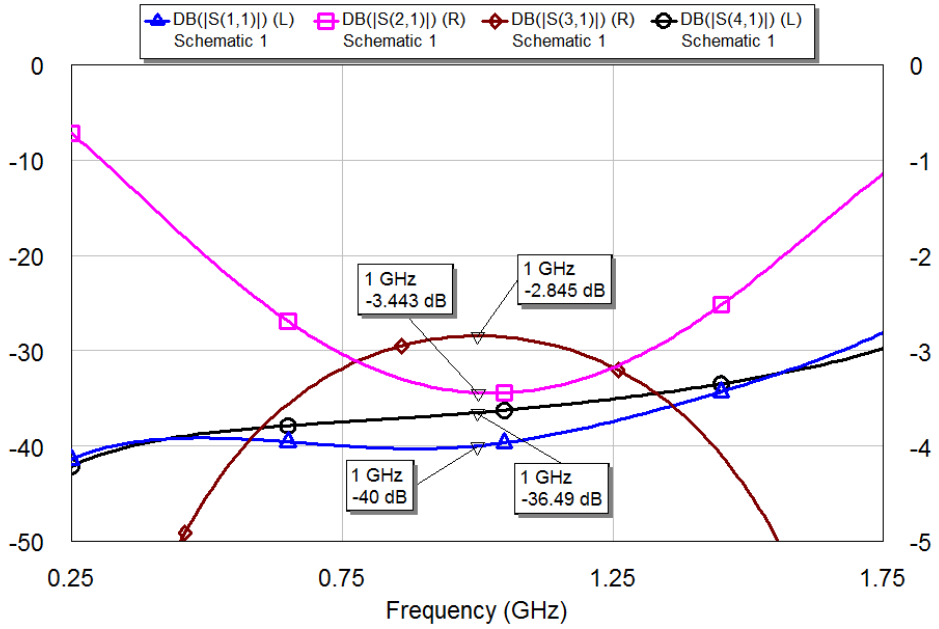

Figure 18: S-parameters for simplest AWR model shown in Fig. 17 with $|S_{11}|$ and $|S_{41}|$ are on the left hand axis while $|S_{21}|$ and $|S_{31}|$ are on the right hand axis. The 3 dB coupler has isolation and return loss below 30 dB, specific values are shown by the markers.

A more realistic AWR model of the coupler is shown in Fig. 19 where vias and extensions of transmission lines (ports and matching sections) are modeled with capacitors and inductors. The vias and extra transmission lines were optimized first.

The values for the vias have an inductance of 620 nH and capacitance of 0.032 pF, the extra transmission lines have an inductance of 0.06 nH and capacitance of 0.032 pF. This indicates the optimal length of transmission line is as small as possible while the optimal size of the via will not be restricted by fabrication tolerances but separation between the lines.

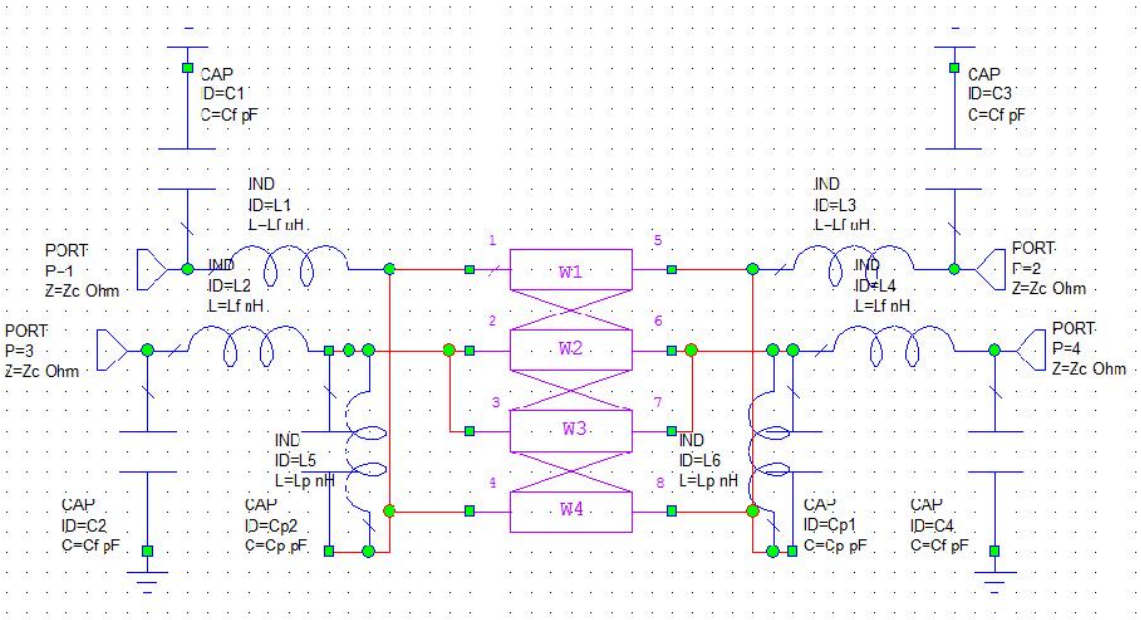

Figure 19: 2D simulation of coupler, similar to Fig. 17 with additional components to take the inductive and capacitive characteristics of both the vias and extra transmission lines into account.

Once the 2D model was optimized, physical restrictions for a 3D topology had to be implemented. The ports had to be separated so that soldered SMA connectors would not touch, the separation between lines had to be larger than the minimum trace size, and extra vias to ground were introduced to deter unwanted coupling. Fig. 20a is a layout of the final design from CST. The figure only shows two of the four ports, the other two ports are at the end of some length L and a mirror image of the one pictured. Fig. 20b is a photograph of the 1 GHz and 3 GHz couplers,

respectively, labeled with length and shown with soldered SMA connectors. The only dimension that changes between the 1 GHz and 3 GHz couplers is the length, all other dimensions stay consistent and are listed in Table 6.

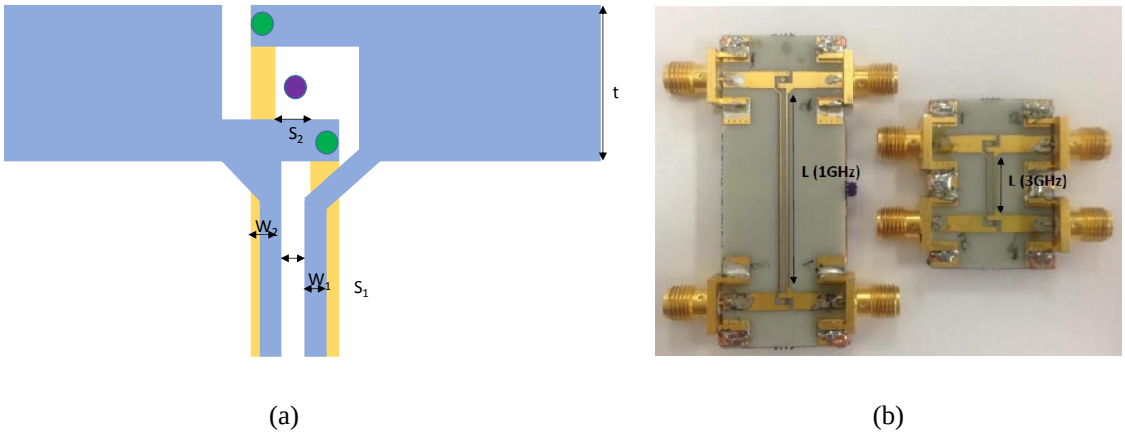

(a) (b)

Figure 20: The dimensions labeled are in Table 6 (a) The layout of one end of the coupler with blue for the top layer, purple for vias to ground, green for vias between first and second layer, and yellow for second layer. (b) Both fabricated couplers for 1 GHz (left) and 3 GHz (right) pictured with SMA connectors used for measurement. The only dimension that changes between the two couplers is their length.

Table 6: Fabricated coupler dimensions corresponding to those labeled in Fig. 20. All dimensions stay the same as frequency shifts except for the length.

Dimension	**Length(mm)**
s_1	0.5
s_2	0.45
w_1	0.2
w_2	0.42
t	1
L (1 GHz)	35
L (3 GHz)	10

In the two following sections simulated and measured results for the coupler depicted in Fig. 20 for both 1 GHz ad 3 GHz are summarized.

4.2.2 Measurement

The measurement set-up includes a two-port VNA (N 5224A) rated from 10 MHz to 43.5 GHz, the coupler, and two fifty-ohm loads. The symmetry of the system indicates any of the ports pictured in Fig. 20 can be assigned as port 1 as long as the other ports follow the order show in Fig. 21. Port 1 is always connected to the VNA, ports 2, 3, and 4 are either terminated in a load or connected to the other port of the Network Analyzer.

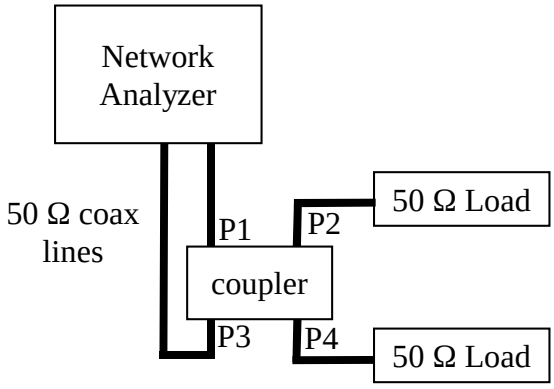

Figure 21: Experimental set-up used to measure the S-parameters of the coupler. The Network Analyzer (N5224A) is connected using 50 Ω coaxial lines to two of the four ports on the coupler. The other two ports are connected to 50 Ω loads.

The measured S-parameters of the first design are shown in Fig. 22. The 1-GHz coupler was measured to have 3 dB coupling and insertion loss, 22 dB isolation and return loss. Meanwhile, the 3 GHz coupler had 3 dB coupling, 20 dB isolation, and 24 dB return loss. The small dB difference between the isolation and return loss is an indication of slight asymmetries within the system.

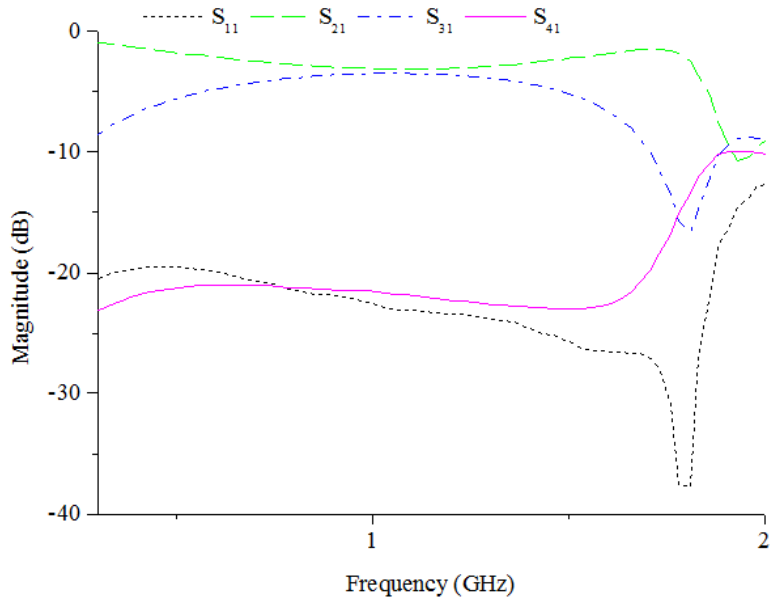

(a)

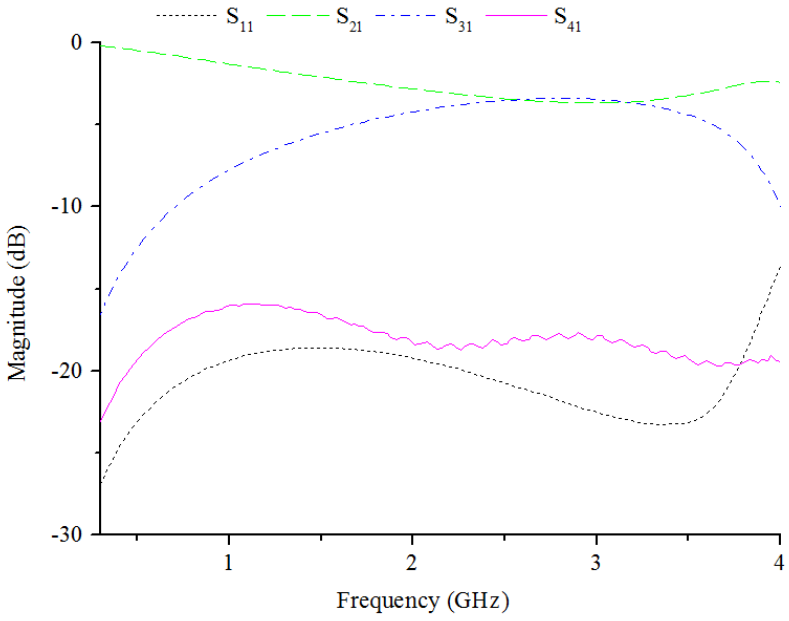

(b)

Figure 22: The measured S-parameters for the first design of the 1 GHz and 3 GHz coupler. All of these measurements were done using the standard calibration described earlier in this chapter. (a) 1 GHz, 3 dB coupler with -22 dB isolation and return loss. (b) 3 GHz, 3 dB coupler with -20 dB isolation and -24 dB return loss.

Unlike the simulations, the fabricated coupler did not have infinite ground, it only had 0.5 oz. of copper on the third layer. This affected the measured results and more ground had to be added in the form of copper tape to keep the coupler stable. There were already through vias to connect the pads so the two grounds did not form a capacitor.

As seen in Fig. 20, the only parameter that has changed between the 1 GHz and 3 GHz coupler is the length. However, electrically speaking a few things have changed as we scaled from 1 to 3 GHz:

- The thickness of the dielectric between the three layers has changed slightly both in electrical length and permittivity. This affects impedance of the 50 Ω port.
- The widths and separations are now electrically larger and will alter the even and odd mode impedances slightly.

The question is if the design compensated for these electrical changes. Fig. 22 shows very similar S-parameters for both frequencies and indicates that these electrical changes have not affected the design. The next design will look into balancing the higher frequencies and improving the isolation.

4.2.3 Discussion

In order to better quantify the design, simulation and measurement are compared and discussed. Their match in terms of amplitude, shape, and bandwidth are considered. The coupler's sensitivity is test given 5% and 10% fabrication tolerances to verify that the measurement results are within scope.

4.2.3.1 Simulation vs. Measurement

Figures 23 and 24 show the S-parameters for measurement vs. simulation. There are three simulations present, two AWR and one CST. The first AWR simulation, using

the setup pictured in Fig. 17, while the second simulation AWR simulation incorporated addition impedances, as shown in Fig. 19.

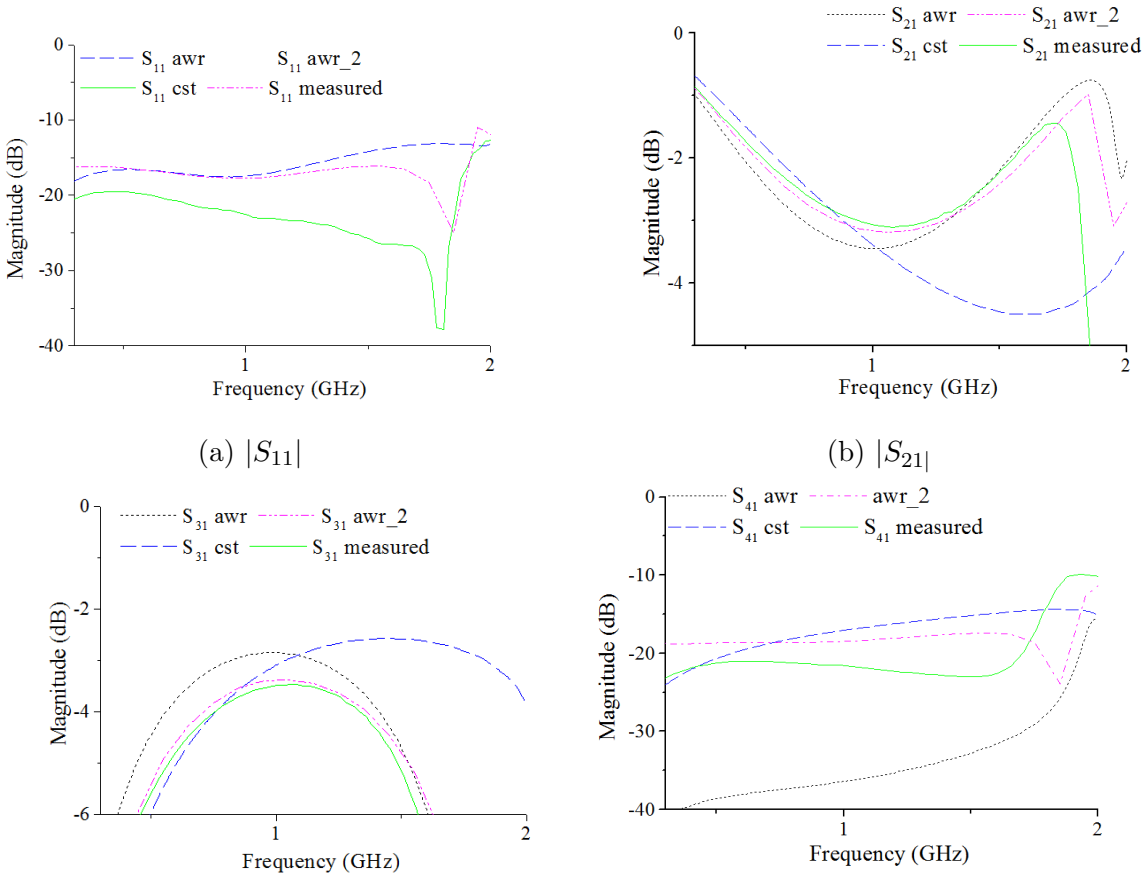

(a) $|S_{11}|$ (b) $|S_{21}|$

(c) $|S_{31}|$ (d) $|S_{41}|$

Figure 23: Simulation of awr and cst vs. measurement for the S-parameters of the 1 GHz coupler for the first coupler design. The first design in AWR, corresponding to Fig. 17 is designated with a dark black dotted line, the second design in awr, shown in Fig. 19 is the dashed dotted magenta line CST with a dashed blue line, and measured with a solid green line.

The initial AWR simulation has a similar shape as the measurement but differing magnitude, this is expected because of the lack of impedances in the simulation model. Once addition impedances in the system were added (ports and vias), the

secondary AWR simulation has a much better match with both shape and magnitude compared to measurement. The magnitude of coupling and isolation loss match well for both simulation and measurement, however CST has both an elongated bandwidth and slight frequency shift. Although the measurement and simulation do not agree perfectly, the measurement fits well between simpler and more complex simulation tools.

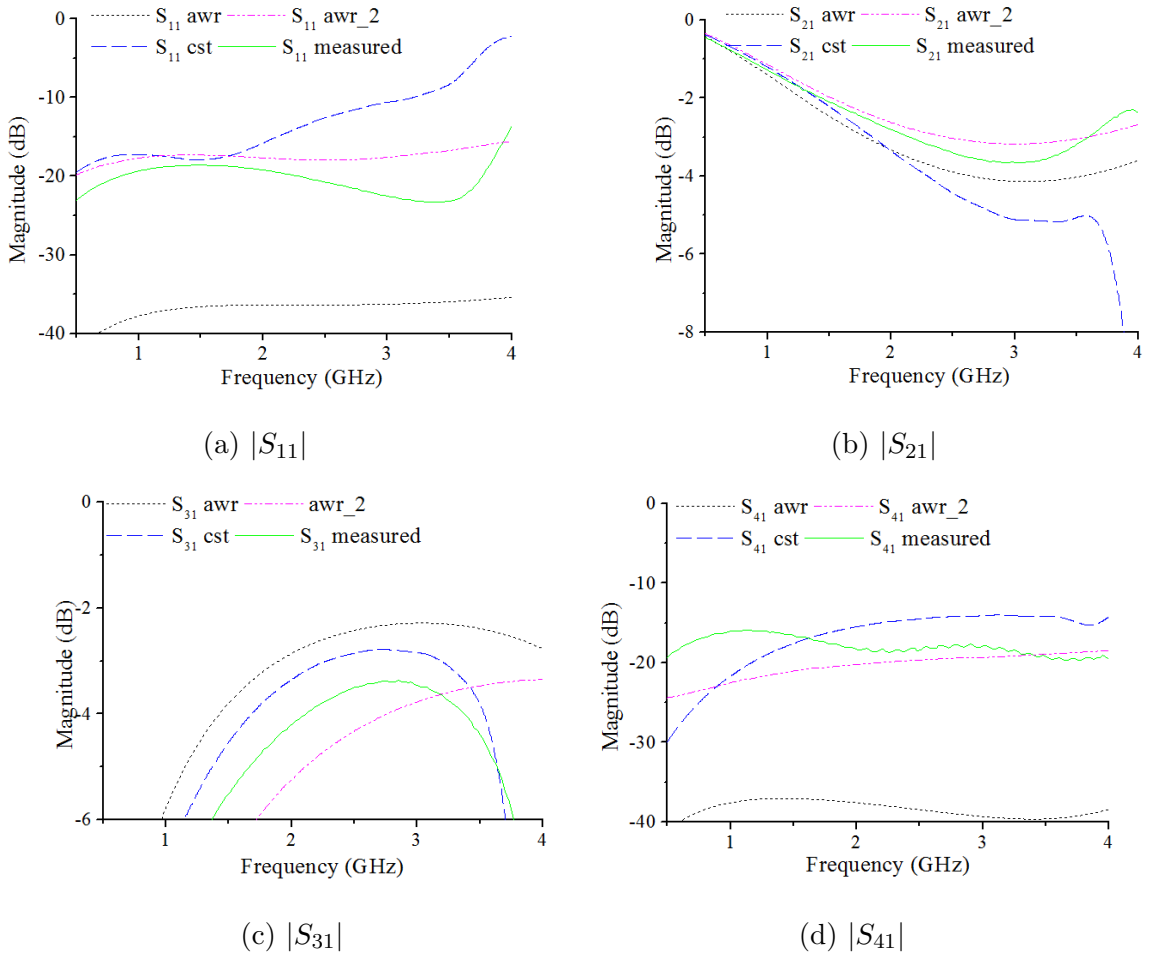

(a) $|S_{11}|$ (b) $|S_{21}|$

(c) $|S_{31}|$ (d) $|S_{41}|$

Figure 24: Simulation of awr and cst vs. measurement for the S-parameters of the 3 GHz coupler for the first coupler design. The first design in AWR, corresponding to Fig. 17 is designated with a dark black dotted line, the second design in awr, shown in Fig. 19 is the dashed dotted magenta line CST with a dashed blue line, and measured with a solid green line.

The initial AWR simulation has similar comparison trends as the 1 GHz trends with same shape and more-ideal amplitudes. The second AWR simulation, which takes additional impedances into account, has similar amplitude but elongated wavelength compared to the measured values for S_{21} and S_{31}. CST no longer has a frequency shift for coupling and insertion loss and matches measurement well in terms of amplitude and shape for all four S-parameters.

Overall both the 1 GHz and 3 GHz coupler have measured values within 10% of CST and the second AWR simulations.

4.2.3.2 Fabrication Tolerances

The dimensional tolerances was studied using the full wave model simulation CST. Several parameters were changed by ±5% and ±10% including; dielectric thickness, copper thickness, separation widths, via size, and the borders of the coupler (milling precision). Figures 25 and 26 show the fabrication tolerances of the coupler for 1 GHz and 3 GHz respectively.

Figures 25 and 26 graph the nominal values of each of the S-parameters against the simulated S-parameters. Each of the points represents the S-parameters at the center frequency of the coupler, the bandwidth changes minimally (largest variation of about 0.01 GHz) with changes in tolerances.

The 1 GHz coupler shows good tolerances to dimensions and permittivity for both 5% and 10% changes to physical parameters. S_{11} and S_{41} are slightly more sensitive to dimension changes, with a dB differing by only by a few dB, while S_{31} and S_{21} shift by less than dB. All four S-parameters are most sensitive when the milling precision and separation widths are increase or decrease by 5% and 10%.

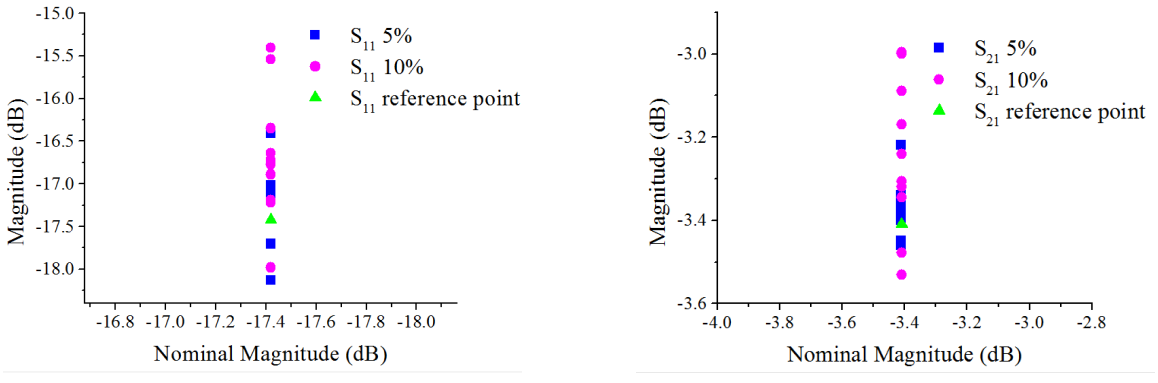

(a) $|S_{11}|$

(b) $|S_{21}|$

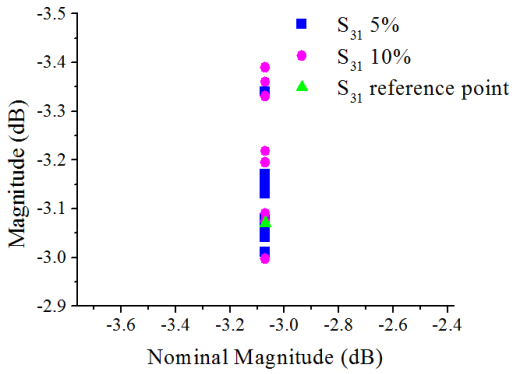

(c) $|S_{31}|$

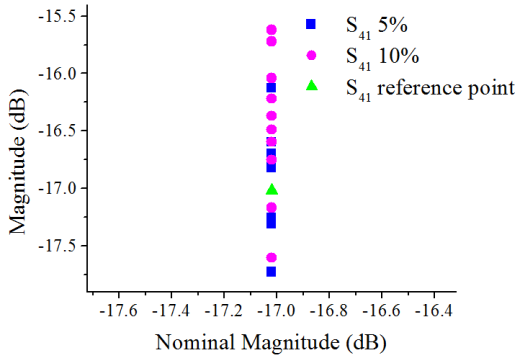

(d) $|S_{41}|$

Figure 25: Evaluating the sensitivity of the 1 GHz coupler by adjusting different parameters of the coupler by 5% and 10%. The blue squares indicates parameters were altered by 5%, the pink circles are the S-parameters after 10% alteration, and the green triangle is the original data s-parameter value. S_{21} and S_{31} are both differ by less than 1 dB while S_{11} and S_{41} differ by only a few %.

The 3 GHz coupler shows similar responses to the 1 GHz coupler for its fabrication tolerance. The outer limits of the fabrication limits, like for the 1 GHz coupler were established by the designs sensitivity to milling precision and separation widths.

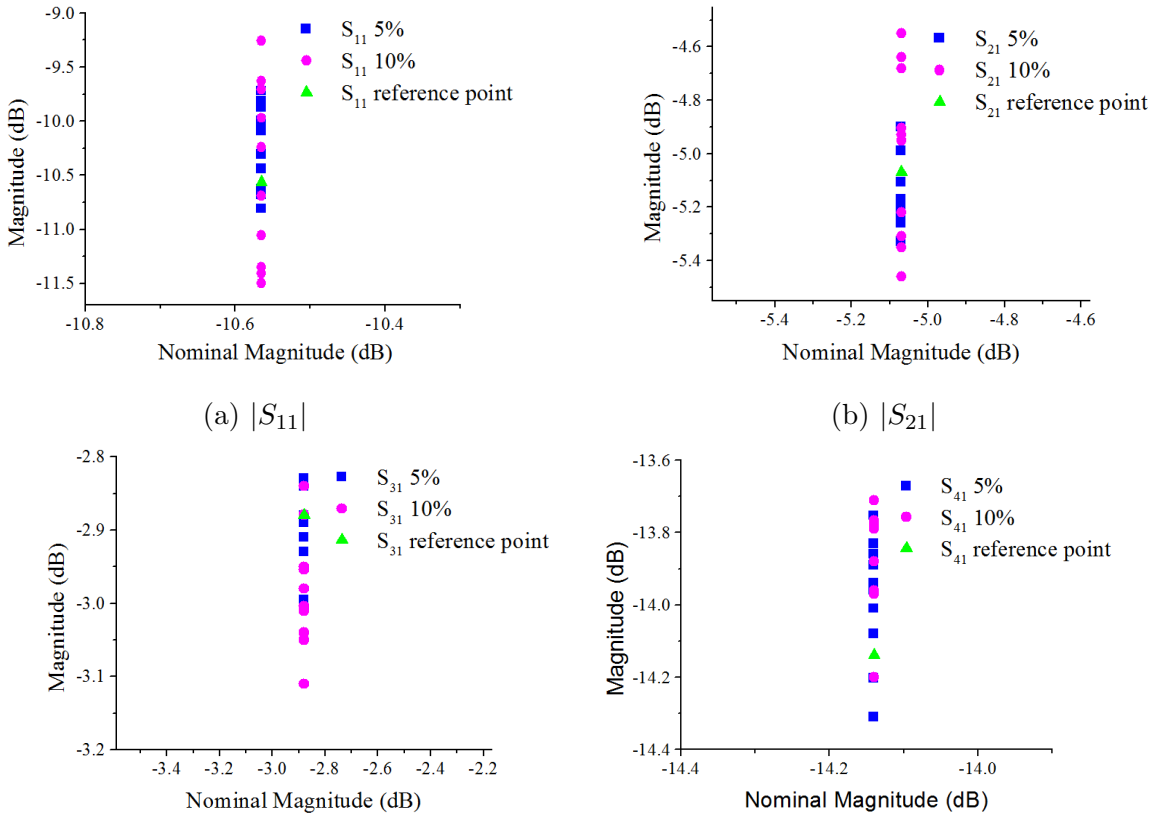

(a) $|S_{11}|$ (b) $|S_{21}|$

(c) $|S_{31}|$ (d) $|S_{41}|$

Figure 26: Evaluating the stability of the 3 GHz coupler by adjusting different parameters of the coupler by 5% and 10%. The blue squares indicates parameters were altered by 5%, the pink circles are the S-parameters after 10% alteration, and the green triangle is the original data s-parameter value.

The sensitivity of both 1 GHz and 3 GHz couplers holds under fabrication tolerances of 5% and 10%. All of the changes to physical parameters were applied equally to all layers, e.g. when the separation was adjusted by 5% both the top and bottom layers were decrease and increased by 5%.

Chapter V

CONCLUSIONS AND FUTURE WORK

The coupler designed, simulated, fabricated, and measured in this thesis achieved the S-parameters, summarized in Table 7, showing that they are comparable to the initial goal presented in Chapter 1. The coupler was able to scale from 1 GHz to 3 GHz but only adjusting the length of the of coupled line sections with small variations in isolation and return loss.

Table 7: Measured characteristic S-parameters of the coupler.

S-Parameter	**Physical Meaning**	**1 GHz**	**3 GHz**
$-20\log\|S_{11}\|$	return loss	-22 dB	-20 dB
$-20\log\|S_{21}\|$	through transmission	-3 dB	-3 dB
$-20\log\|S_{31}\|$	coupling factor	-3 dB	-3 dB
$-20\log\|S_{41}\|$	isolation	-22 dB	-24 dB

Compared to other coupler, such as the branch-line and Lange couplers the multi-layer couplers offer better S-parameters, less loss, and smaller total area. With a similar substrate setup: 1.6mm thick dielectric with a permittivity of 3.66, the length of a 50 Ω line is 44 mm with a width of 3 mm.

An area for future work includes an improved calibration so that the loss of the coupler can also be properly characterized, as well as the phase and amplitude balance. SOLT is not the correct calibration for this measurement, however there are two methods that could be implemented instead; power calibration and a Thru-Reflect-Line (TRL) calibration.

Power measurement could be useful to find the reflected power (P1) at port 1,

transmitting power (P2) at port 2, coupled power (P3) at P3, and power leaking (P4) at the isolated port, P4. From these power measurements the isolation (P4/P1), coupling (P3/P1), and return loss (Pin-P1). Fig. 27 is a simple diagram of how this power measurement would be calibration. With a source attached to a coupler with known characteristics, a power meter attached to the port of interest (port 1 for reflected power, port 2 for transmitting power etc.), and loads attached to all other ports.

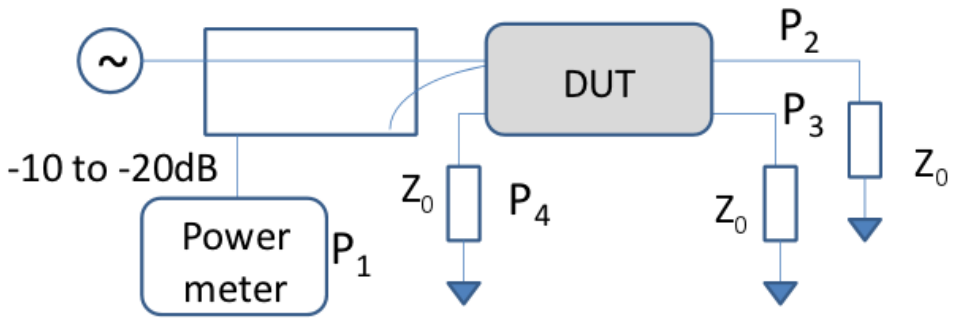

Figure 27: Schematic of power measurement calibration. With the device under testing (DUT) attached to a power source at port 1, power meter attached to port 1 to measure P1, and all other ports terminated in Z_0.

The TRL would require fabricating multi-layer TRL standards in the same substrate configuration as the coupler, since a coaxial SOLT calibration does not calibrate out the errors due to the SMA connector-to-microstrip transition, making precise measurements a challenge. This would also allow phase measurements that are relevant to coupler performance and were not extensively discussed in the thesis in the context of the multi-core interconnect.

Another area of future work is scaling the coupler to higher frequencies using the same fabrication technology and comparing couplers design for 1, 2, and 5 GHz. When this coupler is designed, there is further work to be done also in terms of

more detailed tolerance studies. Although the initial tolerance analysis presented in Chapter 4 gives useful indications in terms of coupler sensitivity to dimensions, a more extensive study that includes connector placement, port geometry, etc. would be useful from a practical standpoint.

Finally, the motivating application of the coupler presented in this thesis are multi-core processor interconnect networks that are directly fabricated on-chip using standard semiconductor processes. Couplers fabricated in such a technology have been presented in e.g. [38] and a similar design of the 3-layer 4-line coupler from this thesis can therefore be implemented in silicon. This thesis describes the method that would allow the design and optimization process to be carried out in any such process.

REFERENCES

[1] Agilent, T., "Overview on interdigital capacitor design." `http://cp.literature.agilent.com/litweb/pdf/5989-8912EN.pdf`. Accessed June 2015.

[2] Akhtarzad, S., Rowbotham, T. R., and Johns, P. B., "The design of coupled microstrip lines," *Microwave Theory and Techniques, IEEE Transactions on*, vol. 23, no. 6, pp. 486–492, 1975.

[3] Akhter, S. and Roberts, J., *Multi-core programming*, vol. 33. Intel press Hillsboro, 2006.

[4] Al-Taei, S., Lane, P., and Passiopoulos, G., "Design of high directivity directional couplers in multilayer ceramic technologies," in *Microwave Symposium Digest, 2001 IEEE MTT-S International*, vol. 1, pp. 51–54, IEEE, 2001.

[5] Bahl, I. J., "Six-finger Lange coupler on 3 mil GaAs substrate using multilayer MMIC technology," *Microwave and Optical Technology Letters*, vol. 30, no. 5, pp. 322–327, 2001.

[6] Chang, C.-P., Chiu, J.-C., Chiu, H.-Y., and Wang, Y.-H., "A 3-dB quadrature coupler using broadside-coupled coplanar waveguides," *Microwave and Wireless Components Letters, IEEE*, vol. 18, no. 3, pp. 191–193, 2008.

[7] Chirala, M. K. and Nguyen, C., "Multilayer design techniques for extremely miniaturized CMOS microwave and millimeter-wave distributed passive circuits," *Microwave Theory and Techniques, IEEE Transactions on*, vol. 54, no. 12, pp. 4218–4224, 2006.

[8] Cohn, S. B., "Characteristic impedances of broadside-coupled strip transmission lines," *Microwave Theory and Techniques, IRE Transactions on*, vol. 8, no. 6, pp. 633–637, 1960.

[9] Dalley, J. E., "A strip-line directional coupler utilizing a non-homogeneous dielectric medium," *Microwave Theory and Techniques, IEEE Transactions on*, vol. 17, no. 9, pp. 706–712, 1969.

[10] Djordjević, A. R., Napijalo, V. M., Olćan, D. I., and Zajić, A. G., "Wideband multilayer directional coupler with tight coupling and high directivity," *Microwave and Optical Technology Letters*, vol. 54, no. 10, pp. 2261–2267, 2012.

[11] Edwards, T. C., *Foundations for microstrip circuit design*. John Wiley & Sons Canada, Limited, 1992.

[12] Garg, R. and Bahl, I. J., "Characteristics of coupled microstriplines," *Microwave Theory and Techniques, IEEE Transactions on*, vol. 27, no. 7, pp. 700–705, 1979.

[13] Geer, D., "Chip makers turn to multicore processors," *Computer*, vol. 38, no. 5, pp. 11–13, 2005.

[14] Gepner, P. and Kowalik, M. F., "Multi-core processors: New way to achieve high system performance," in *Parallel Computing in Electrical Engineering, 2006. PAR ELEC 2006. International Symposium on*, pp. 9–13, IEEE, 2006.

[15] Ghali, H. and Moselhy, T. A., "Miniaturized fractal rat-race, branch-line, and coupled-line hybrids," *Microwave Theory and Techniques, IEEE Transactions on*, vol. 52, no. 11, pp. 2513–2520, 2004.

[16] Ghione, G. and Naldi, C. U., "Coplanar waveguides for MMIC applications: Effect of upper shielding, conductor backing, finite-extent ground planes, and line-to-line coupling," *Microwave Theory and Techniques, IEEE Transactions on*, vol. 35, no. 3, pp. 260–267, 1987.

[17] Ghorbanzade, P., "Analysis, Design and Simulation of an X-Band Moreno Crossed-Waveguide Directional Coupler," 2013.

[18] Gruszczynski, S., Wincza, K., and Sachse, K., "Design of high-performance three-strip 3-DB directional coupler in multilayer technology with compensated parasitic reactances," *Microwave and Optical Technology Letters*, vol. 49, no. 7, pp. 1656–1659, 2007.

[19] Gu, J. and Sun, X., "Miniaturization and harmonic suppression rat-race coupler using C-SCMRC resonators with distributive equivalent circuit," *Microwave and Wireless Components Letters, IEEE*, vol. 15, no. 12, pp. 880–882, 2005.

[20] Healy, M. B., Athikulwongse, K., Goel, R., Hossain, M. M., Kim, D. H., Lee, Y.-J., Lewis, D. L., Lin, T.-W., Liu, C., Jung, M., and Others, "Design and analysis of 3D-MAPS: A many-core 3D processor with stacked memory.," in *CICC*, pp. 1–4, 2010.

[21] Hirota, T., Minakawa, A., and Muraguchi, M., "Reduced-size branch-line and rat-race hybrids for uniplanar MMIC's," *Microwave Theory and Techniques, IEEE Transactions on*, vol. 38, no. 3, pp. 270–275, 1990.

[22] Ho, C.-H., Fan, L., and Chang, K., "Broad-band uniplanar hybrid-ring and branch-line couplers," *Microwave Theory and Techniques, IEEE Transactions on*, vol. 41, no. 12, pp. 2116–2125, 1993.

[23] Horno, M. and Medina, F., "Multilayer planar structures for high-directivity directional coupler design," *Microwave Theory and Techniques, IEEE Transactions on*, vol. 34, no. 12, pp. 1442–1449, 1986.

[24] Hsu, C.-L., Kuo, J.-T., and Chang, C.-W., "Miniaturized dual-band hybrid couplers with arbitrary power division ratios," *Microwave Theory and Techniques, IEEE Transactions on*, vol. 57, no. 1, pp. 149–156, 2009.

[25] Instruments, N., "Awr software tool." `http://www.awrcorp.com/`. Accessed August 2014 - July 2015.

[26] Javadzadeh, S. M. H., Majedi, S. M. S., and Farzaneh, F., "Broadside Coupler Channels 1 to 10 GHz," *Microwaves and RF*, vol. 51, 2012.

[27] Kim, D., Choi, Y., Allen, M. G., Kenney, J. S., and Kiesling, D., "A wide bandwidth monolithic BST reflection-type phase shifter using a coplanar waveguide Lange coupler," in *Microwave Symposium Digest, 2002 IEEE MTT-S International*, vol. 3, pp. 1471–1474, IEEE, 2002.

[28] Klein, J. L. and Chang, K., "Optimum dielectric overlay thickness for equal even-and odd-mode phase velocities in coupled microstrip circuits," *Electronics Letters*, vol. 26, no. 5, pp. 274–276, 1990.

[29] Kundu, M. K., *Advanced Computing, Networking and Informatics, Volume 2: Wireless Networks and Security Proceedings of the Second International Conference on Advanced Computing, Networking and Informatics (Icacni-2014)*. Smart Innovation, Systems and Technologies, Springer, 2014.

[30] Lange, J., "Interdigitated stripline quadrature hybrid (correspondence)," *Microwave Theory and Techniques, IEEE Transactions on*, vol. 17, no. 12, pp. 1150–1151, 1969.

[31] Levy, R., "Analysis and synthesis of waveguide multiaperture directional couplers," *Microwave Theory and Techniques, IEEE Transactions on*, vol. 16, no. 12, pp. 995–1006, 1968.

[32] Li, K., Kurita, D., and Matsui, T., "An ultrawideband bandpass filter using broadside-coupled microstrip-coplanar waveguide structure," in *Microwave Symposium Digest, 2005 IEEE MTT-S International*, pp. 4—-pp, IEEE, 2005.

[33] Mahon, J. P. and Elliott, R. S., "Tapered transmission lines with a controlled ripple response," *Microwave Theory and Techniques, IEEE Transactions on*, vol. 38, no. 10, pp. 1415–1420, 1990.

[34] Microwaves101, "Klopfenstein taper." `www.microwaves101.com`. Accessed May-July 2015.

[35] Microwaves101, "Lange coupler." `www.microwaves101.com`. Accessed May-July 2015.

[36] Moscoso-Martir, A., Molina-Fernandez, I., and Ortega-Monux, A., "High performance multi-section corrugated slot-coupled directional couplers," *Progress In Electromagnetics Research*, vol. 134, pp. 437–454, 2013.

[37] Napijalo, V. and Kearns, B., "Multilayer 180 coupled line hybrid coupler," *Microwave Theory and Techniques, IEEE Transactions on*, vol. 56, no. 11, pp. 2525–2535, 2008.

[38] Nasr, I., Nehring, J., Aufinger, K., Fischer, G., Weigel, R., and Kissinger, D., "Single-and Dual-Port 50-100-GHz Integrated Vector Network Analyzers With On-Chip Dielectric Sensors," 2014.

[39] Oh, J., Zajic, A., and Prvulovic, M., "Traffic steering between a low-latency unswitched TL ring and a high-throughput switched on-chip interconnect," in

Proceedings of the 22nd international conference on Parallel architectures and compilation techniques, pp. 309–318, IEEE Press, 2013.

[40] Okazaki, H. and Hirota, T., "Multilayer MMIC broad-side coupler with a symmetric structure," *Microwave and Guided Wave Letters, IEEE*, vol. 7, no. 6, pp. 145–146, 1997.

[41] Oshpark. `https://oshpark.com/`. Accessed August 2014 - July 2015.

[42] Pan, B., Yoon, Y., Zhao, Y. Z., Papapolymerou, J., Tentzeris, M. M., and Allen, M., "A broadband surface-micromachined 15-45 GHz microstrip coupler," in *IEEE MTT-S International Microwave Symposium Digest*, vol. 2005, pp. 989–992, IEEE, 2005.

[43] Phromloungsri, R., Chongcheawchamnan, M., and Robertson, I. D., "Inductively compensated parallel coupled microstrip lines and their applications," *Microwave Theory and Techniques, IEEE Transactions on*, vol. 54, no. 9, pp. 3571–3582, 2006.

[44] Pozar, D. M., *Microwave Engineering, 4th Edition*. Wiley Global Education, 2011.

[45] Ramanathan, R. M., "Intel{\textregistered} Multi-Core Processors," *Making the Move to Quad-Core and Beyond*, 2006.

[46] Riblet, H. J. and Saad, T. S., "A new type of waveguide directional coupler," *Proceedings of the IRE*, vol. 36, no. 1, pp. 61–64, 1948.

[47] Sawicki, A. and Sachse, K., "A novel directional coupler for PCB and LTCC applications," in *Microwave Symposium Digest, 2002 IEEE MTT-S International*, vol. 3, pp. 2225–2228, IEEE, 2002.

[48] Simons, R. N., *Coplanar waveguide circuits, components, and systems*, vol. 165. John Wiley & Sons, 2004.

[49] software tool, C. `https://www.cst.com/`. Accessed August 2014 - July 2015.

[50] Tajima, Y. and Kamihashi, S., "Multiconductor couplers," *Microwave Theory and Techniques, IEEE Transactions on*, vol. 26, no. 10, pp. 795–801, 1978.

[51] Tang, C. W. and Chen, M. G., "Design of multipassband microstrip branch-line couplers with open stubs," *IEEE Transactions on Microwave Theory and Techniques*, vol. 57, no. 1, pp. 196–204, 2009.

[52] Tefiku, F., Yamashita, E., and Funada, J., "Novel directional couplers using broadside-coupled coplanar waveguides for double-sided printed antennas," *Microwave Theory and Techniques, IEEE Transactions on*, vol. 44, no. 2, pp. 275–282, 1996.

[53] Toyoda, I., Hirota, T., Hiraoka, T., and Tokumitsu, T., "Multilayer MMIC branch-line coupler and broad-side coupler," in *Microwave and Millimeter-Wave Monolithic Circuits Symposium, 1992. Digest of Papers, IEEE 1992*, pp. 79–82, IEEE, 1992.

[54] TriQuint, S., "Lange coupler set tgb2001." `http://www.triquint.com/`. Accessed June 2015.

[55] Tyrrell, W. A., "Hybrid circuits for microwaves," *Proceedings of the IRE*, vol. 35, no. 11, pp. 1294–1306, 1947.

[56] Weiss, J. A., Bryant, T. G., and Saad, T. S., "Microwave engineer's handbook," 1971.

[57] Wen, C. P., "Coplanar-waveguide directional couplers," *Microwave Theory and Techniques, IEEE Transactions on*, vol. 18, no. 6, pp. 318–322, 1970.